Quantitative characterization of microbial communities micro-biogeography during infectious disease.

A Dissertation
Presented to
The Academic Faculty

by

Juan P Barraza

In Partial Fulfillment
of the Requirements for the Degree
Doctor of Philosophy
in the
School of Biological Sciences

Georgia Institute of Technology
December 2021

Quantitative characterization of microbial communities micro-biogeography during infectious disease.

Approved by:

Dr. Marvin Whiteley, Advisor
School of Biological Sciences
Georgia Institute of Technology

Dr. William Ratcliff
School of Biological Sciences
Georgia Institute of Technology

Dr. Sam Brown
School of Biological Sciences
Georgia Institute of Technology

Dr. Peter Yunker
School of Physics
Georgia Institute of Technology

Dr. Brian Hammer
School of Biological Sciences
Georgia Institute of Technology

Date Approved: September 22nd, 2021

ACKNOWLEDGEMENTS

I would like to the the Center for Microbial Dynamics, and the Georgia Tech community at large, for welcoming me in to the department and promoting engagement in insightful discussion and scientific discovery. Particular thanks for my friends in the center, for helping me enjoy science inside and outside the lab.

I would also like to thank all of the members of the Whiteley lab I ever interacted. A fundamental reason I joined the Whiteley lab , was the increadibly high quality of people it attracts and harbors. Special thanks to Dan, for promoting a constant insifgtful discussion about science inside and outside academia and to Marvin, for setting the standard for what it is to be a great scientist and providing an environment where I have grown in several aspects of life.

Finally, I thank Joaquin Avellan, for helping me develop a passion for microbial communities and their impact on human lives and my family and friends for their constant cheerful support.

TABLE OF CONTENTS

LIST OF FIGURES

LIST OF SYMBOLS AND ABBREVIATIONS

Aa	*Aggregatibacter actynomycetemcomitans*
HQNO	2-heptyl-4-quinolinol 1-oxide
SCFM2	Synthetic cystic fibrosis sputum
Sg	Streptococcus gordonii
μm3	micrometer

SUMMARY

Spatial structure, the arrangement of organisms in space, is an essential feature of life. It provides a mechanism for speciation, promotes niche development and shapes community function. Many methods exist to characterize the spatial structure of communities of animals and plants, but few exist for microbial communities, which impact many aspects of life, including human health. Interactions between microbes within a community during infection often result in increased tolerance to antibiotics and worse clinical outcomes. My thesis draws upon techniques from molecular biology, fluorescence microscopy, community ecology and computer science to build a framework to quantitatively characterize the spatial structure of microbial communities at the micron scale and aims to characterize bacterial interactions during infection and their impact on human health.

Interactions can be broadly classified as competitive or cooperative, and I use two different infection models to explore each one. To observe the impact competitive interactions, I use a model community of *P. aeruginosa* and *S. aureus* in a mouse chronic wound infection model. These two microbes co-exist in many infections, but most of their characterized interactions involve growth inhibition and killing. To observe the impact of cooperative interactions, I use *Streptococcus gordonii* and *Aggregatibacter actinomycetemcomitans* in a mouse abscess model. These two microbes co-exist in the oral cavity and exchange nutrients, including lactate, to grow more effectively. By capturing images of these bacterial communities during infection and analyzing them, we identify how interactions within microbial communities impact the aggregation, abundance, and distribution in space of its members. Specifically, *P. aeruginosa*-secreted antimicrobial HQNO increases the

number of planktonic cells in *S. aureus* and increases the micron-scale enrichment distance between these two microbes. We also show that lactate released by *S. gordonii* reduces the micron-scale enrichment distance between *S. gordonii* and *A. actinomycetemcomitans*. Overall, this works focused on developing tools for the exploration of micron-scale spatial structure and its impact on bacterial physiology during infection.

CHAPTER 1. INTRODUCTION

Spatial structure, the arrangement of organisms in space, is an essential feature of life. It provides a mechanism for speciation, promotes niche development and shapes community function. Many methods exist to characterize the spatial structure of communities of animals and plants, but few exist for microbial communities. Microbes often exist in highly complex, dynamic, and diverse communities(1-3) and understanding interactions within these communities is crucial for many aspects of life(4), including human health(5, 6). The work described here draws upon techniques from molecular biology, fluorescence microscopy, community ecology and computer science to build a framework to quantitatively characterize the spatial structure of microbial communities at the micron scale. The intention is to find mechanisms of bacterial interactions and identify their impact on human health, with an emphasis on infectious diseases. This chapter provides context for this work by 1) describing the impact of spatial structure in the understanding of biological systems, 2) giving an overview of microbial interactions, and 3) how these two themes can come together to answer basic questions about infectious diseases.

1.1 Spatial Structure of Biological Systems

1.1.1 Defining Microbiogeography

Biogeography studies the distribution patterns of organisms across space and time and the factors that determine those patterns (7-9). Work in this field has primarily used observations from plants and animals to develop models to explain phenomena occurring

at scales that range from small habitats to entire biomes (10-14). However, sequencing technologies have more recently allowed the biogeography of microbes to be studied (9, 15, 16). Early work in microbial biogeography aimed to address the Baas-Becking tenet: "Everything is everywhere, but the environment selects"(17). While the scaling of the organism surveyed changed significantly, the scaling of the surveying area remained, and few conclusions have been drawn from this work. Looking for microbial patterns observed at the scale of macro-organisms might not be relevant for microbes, especially for those exclusive to enclosed environments. My thesis is that the biogeography of micro-scale organisms should include surveys at the micron scale.

Scale can be defined using two components: grain and size. Grain is the size of the individual units of observation and extent is the overall area encompassed by an investigation(18, 19). The values for these parameters are key to understand the goal and intention of work on the biogeography of microbes. The data used to characterize biogeography in the work described here primarily comes from microscopy images. Thus, the grain is in the tenths of microns and ultimately defined by the pixel size of the microscopy image. The extent is the size of the image, which is in the hundreds of microns. Thus, I will refer to the biogeography of microbes within that grain and extent as *microbiogeography*, a term not currently defined in the literature, but necessary to describe the microbes acting on their local environment and to discriminate from previous work on microbial biogeography. The patterns that microbes may form at this scale are dominated by diffusion, which acts on this scale, and might better provide a mechanistic understanding for them.

1.1.2 Patterns and Scale

The issue of pattern and scale is considered a fundamental problem in biology(19-21). In essence, it describes how a pattern observed at a specific scale may provide a mechanism that affects the dynamics of another scale. This enables the observer to understand the system as a whole and make general predictions. Several examples exist on this effect in macro-ecology(22, 23). In molecular microbiology, this issue arises when a phenotype decreases the fitness of an individual. For instance, when an amino acid within an enzyme changes, the rearrangement at the atomic level can affect enzymatic activity and thus, the phenotype of the cell carrying this protein. While the individual cell and the atom operate at different scales, their fates are inherently tied. Thus, in the context of infectious diseases, the exploration of microbiogeography can identify mechanisms from patterns observed at the scale of microbes that lead to a better understanding and making predictions about the infection as a whole(1). Current efforts to characterize microbiogeography include a recent description of three levels of scale implicated in oral plaque: the macroscale, concerned with 1 mm to 1 cm or more and involved with colonized human structures; the microscale spanning 1 to 10 μm, the size of the cells; and the mesoscale, which spans from 10 to 100 μm and is where diffusion effects and groups of cells are observed(18). Below, I will describe some examples of spatial structure patterns that have been observed in biological systems.

1.1.2.1 Species-abundance patterns

The species-abundance pattern answers the question: how many members of a species are in a community? Extending this question to all species describes the

biodiversity of a community. A common characteristic observed in communities at the macro-scale is a massive disparity in abundance across different species(24). Specifically, that most organisms in a community belong to very few species(25-27). However, environments allowing the formation microenvironments can promote a more even distribution of species(28). Several microbiome studies support this effect, showing few taxa dominating in both environmental and human-associated communities(29-33). Ultimately, two features of microbes may help better understand the species- abundance patterns: the ability to sample every individual in a community and using genetic manipulation of microbes to selectively remove functions and directly explore a mechanistic understanding of the observed patterns.

The occupancy-abundance relationship also describes the tendency of abundant taxa in one community to also be the most widespread species(34). The more environments a species is found in, the more abundant that species is in those environments. While there are many factors that contribute to this effect, the mechanism for this relationship is still poorly understood. There is some evidence that this relationship also applies to microbes in several microbial communities. In the context of infectious disease, *Pseudomonas aeruginosa* and *Staphylococcus aureus* are both as cosmopolitan as humans(35) and found at high densities in polymicrobial infections like the lungs of people with cystic fibrosis and chronic wounds(36-38). These infections are in environments open to many bacterial species and the dominance they exert in the community and associated loss in diversity has been proposed to be hallmarks for disease. This has led to the hypothesis that polymicrobial infections are expected to be dominated by a few microbes, an understanding their

interactions in the context of biogeography can promote our understanding of infectious disease.

1.1.2.2 Turing patterns

Alan Turing described a mathematical basis for simple shapes to transition into more complex structural spatial organizations in 1952 using an embryo as the model (39). The transition proceeds as an interplay between chemical reactions and diffusion of metabolites. While the conditions described in the paper are hard to achieve in nature, reaction-diffusion systems help explain some patterns found in nature. Examples include patterns associated with pigmentation in animals(40-42), and more general in synthetic systems(43), including bacterial communities(44). These systems relate directly to microbiogeography because diffusion plays a major role in motion of organisms and metabolites and modulates interactions at this scale (45-47). Thus, the basis of this principle suggests that reaction-diffusion interactions between microbes can result in patterns found in microbiogeography, and their identification may unravel mechanistic principles in the system.

1.1.2.3 Distance-decay relationship

A basic pattern observed in geography is the distance decay-relationship, which describes the decline of interactions between two organisms as the distance between them increases(24, 48). This concept can be extended to describe an “activity space”, outside of which interactions between organisms decrease dramatically or are negligible. Several studies have used this principle to identify potential interactions between microorganisms at different scales, yet grain size in most of them is on the order of a few centimeters or

larger(24, 49-51). The oral microbiota provides an example on how the distance decay-relationship can be used at the micron scale to advance our understanding of system. Microscopy images from oral samples looking at which organisms are observed in close proximity to one another have paved the way towards the understanding of the ecological succession that occurs during the colonization of the mouth(18, 52-54).

The relevance of this relationship to microbiogeography is multifold. First, it can associate the distance between two organisms, a simple direct measurement, with a magnitude for interactions, something that can be more difficult to quantify. Second, since non-active motion at micron distances is primarily driven by diffusion, spatial arrangements within microbes at the scale of microbiogeography should also be influenced by diffusion. Consequently, while microorganisms that are within diffusion distances may not be interacting, microorganisms outside a diffusion-dictated activity space cannot be interacting directly. Thus, quantifying distances between microorganisms within the microbiogeography scale can serve as a benchmark to quantify interactions between microorganisms.

1.1.2.4 Looking forward

Identifying patterns in microbiogeography, using principles from previous work developed in macro-ecology, might help us understand microbial communities, their interactions, and their impact on disease dynamics. Furthermore, the ability to sample an entire community and use genetics to test mechanisms of interactions opens the door for validation of these patterns, something that is difficult to do at the macro scale. To develop a pattern recognition tool that incorporates the abundance, diffusion, and distance-decay

relationships, I developed the metric "Proportional occupancy." This metric quantifies the density of a species at discrete distance intervals away from another species on a global scale. Kim et al. (55) describes how it can be used to identify the spatial structure required for infection in a human oral community. In Chapters 2, 3 and 4, it is used to identify enrichment distances between two organisms and how they are impacted by the secretion of specific metabolites. The next subsection describes features of microbial biogeography, some of which will be used in later chapters to characterize microbiogeography.

1.1.3 Patterns and scales in microbial communities

Observations of microorganisms and their associated micron-scale patterns are as old as microbiology itself. Antonie van Leeuwenhoek was the first person to observe life at the micron scale. Using high power lenses that he designed and produced, he observed free-floating and motile "animalcules", a term coined from the Dutch to Latin translation of "tiny animals". Using samples from rainwater, ponds, and his mouth, he observed protozoa and oral bacteria. While he had no formal scientific training, he's credited as the first human to visualize a bacterium, immortalized in drawings published in 1683 in the Philosophical Transactions of the Royal Society. Advances in microscopy techniques have allowed us to identify several patterns that are hallmarks for bacterial communities, some of which will be described below. Focus will be on patterns found in host-associated communities.

1.1.3.1 Planktonic cells

Bacterial cells that are free-floating in an environment are referred to as planktonic. The term derives from plankton that have an even distribution in the ocean at large ranges of grain and extent. In the context of this thesis, planktonic cells are defined as bacterial

objects observed via confocal microscopy that are smaller than 5 μm^3s. The impact of planktonic cells in disease remains poorly understood, but they are implicated as the primary etiological agent of acute infections as well as a means of dispersal in chronic infections. Thus, their relative abundance compared to cells in groups may help understand disease pathogenesis.

1.1.3.2 Biofilms

Biofilms are densely packed communities of microbial cells that grow as groups, often attached to surfaces, and surrounded by extracellular polymers that may be self-produced or acquired from the environment. Natural biofilms come in a range of sizes and cell numbers and growth in groups provides emergent properties to their members, including antibiotic resistance, which is particularly important in infectious diseases (56-58). Since the size can vary substantially, the shape of these structures is also highly variable. In vitro, mushroom-shaped complex multicellular structures separated by water-filled spaces have been highly characterized and are the best understood biofilms to date, although their prevalence in infectious disease is still poorly characterized.

In the context of this thesis, I will use the term aggregate to refer to individual groups of bacteria that are larger than 5 μm^3(59). Aggregates have been observed in lung infections of people with cystic fibrosis(60), for which the main pathogens are *P. aeruginosa* and *S. aureus*. Aggregates of *P. aeruginosa* have been characterized *in vitro* and interactions between aggregates via quorum sensing can occur within 200 μm of each other in a recapitulated CF environment(61). The scale at which aggregates interact, and their prominent presence in disease suggest their microbiogeography can impact disease

dynamics. Work described in the following chapters characterizes features of aggregates and planktonic cells in infection and infection-like systems that further our understanding on the life cycle of bacteria, discriminate between chronic and acute infections and identify interactions within microbial communities.

1.1.3.3 Microbial spatial structures found in nature

Microbial communities form specific patterns in host-associated environments, particularly in the oral cavity. Early observations of mouth bacteria showed single layers of cells parallel to each other and perpendicular to a surface, a pattern referred to as "palisade columns."(52) More recent observations using taxon-specific fluorescent probes have shown bacteria of different taxa arranged in concentric circles resembling a "hedgehog" and series of filamentous bacteria with cocci at the ends have been referred to as "corncob structures." (62) Observation of these patterns and shapes have led to an understanding of the physiology and dynamics of the oral microbiota. In a previously published study where I participated, the microbiogeography of communities of the oral bacteria *Streptococcus mutans* and *Streptococcus oralis* impacts their physiology and pathogenesis in humans(55). These patterns have led to better understanding of interactions within the oral community and provided new potential avenues of therapeutic intervention. The next section provides an overview of interactions between microbes and the impact of spatial structure on those interactions.

1.2 Interactions at the Micron Scale:

1.2.1 Overview of microbial interactions

The observation that different bacterial species interact and form discrete spatial structures is relatively new, especially in the context of disease. The formal study of bacteria and their impact in disease was established by Louis Pasteur, who showed that the bacterium *Bacillus anthracis* was responsible for anthrax, a common disease that affected humans and cattle in the XIX century. His work was expanded by Robert Koch, who formalized the association of bacteria and disease in the 1880's into what is known as the "Koch's postulates"(63). It stipulates that the causative agent of an infectious disease is the presence of specific bacteria in a host and, conversely, the removal of that bacteria results in the removal of disease. These criteria proved useful in cementing the acceptance of germ theory and accurately modeled diseases like cholera and anthrax, which led to "the golden age of bacteriology." However, it soon became clear that few diseases follow these criteria, and although Koch's postulates were later reestablished in molecular terms(64), there is growing evidence showing many infectious diseases are either caused or aggravated by interactions between different microbes(5, 65). Therefore, it is essential to consider microbial communities and their interactions to understand infectious diseases. The rest of this section describes the nature of bacterial interactions, specific examples related to infectious diseases, and the impact that spatial structure plays in them.

1.2.2 Ecological interactions between microbes in communities

The outcomes of interactions between organisms generally fall into three categories: positive (+), negative (-) or neutral (0). The pairwise combinations of these three categories are commonly referred to as: mutualism (+,+), competition (-,-), predation (+,-), parasitism (-,+), commensalism (+,0), and amenalism (-,0)(66). While this framework is useful for understanding how specific interactions unfold, organisms can engage in multiple exchanges simultaneously, so the overall relationship between two organisms is the result of a complex network of different types of interactions(67). Below are descriptions of the categories observed in the context of microbiogeography and their impact on disease. The scope of these descriptions is restricted to interactions between microbes of different species and pools together these categories based on the outcome for interacting partners, resulting in either synergistic or hostile interactions.

1.2.2.1 Mutualism (+,+) and commensalism (+,0)

Mutualism describes a situation where both organisms gain a positive outcome from the interaction and commensalism is when only one organism gains a positive outcome while the other is unaffected. These two categories are described together because the overall outcome is positive for the community, which is the most relevant description in the context of infectious disease. This positive outcome of an interaction can also be referred to as "synergy", and in polymicrobial infections, it can be manifested as more aggressive and recalcitrant infections(1). While there are several examples of microbial synergy during infection, the focus will be on antibiotic resistance and cross-feeding.

Antibiotic resistance occurs when a microbe requires a higher dosage of an antimicrobial to be inhibited or killed. This outcome has been observed widely in interspecies biofilm; one example is *P. aeruginosa* and *S. aureus*. These two organisms are found to co-occur in different human chronic infections, and *S. aureus* can tolerate higher doses of tobramycin upon exposure to 2-heptyl-4-hydroxyquinoline-N-oxide (HQNO)(68), a metabolite released by *P. aeruginosa*(69). Chapter 3 describes this effect in detail, and its impact on the spatial organization of this community in an environment that recapitulates CF sputum.

Cross-feeding is when metabolic by-products released by one species are used by another species. The impact of this outcome in bacterial infection relies on the ability of a microbe to obtain nutrients from the microbial community instead of the host. This feature is useful for pathogens, since hosts have mechanisms to sequester nutrients from bacteria, a strategy known as nutritional immunity. A well-studied example of cross-feeding is found within oral microbes. *Streptococcus gordonii* releases L-lactate and *Aggregatibacter actinomycetemcomitans* uses the L-lactate as a preferred carbon source for growing(70, 71). *S. gordonii* also releases hydrogen peroxide (H_2O_2) that *A. actinomycetemcomitans* decomposes into oxygen that it can use for respiration(72). At the scale of infection, these synergistic interactions result in increased virulence during localized abscess infections(65, 70, 72). Chapter 4 describes this interaction in detail and its impact in the spatial organization of this community *in vivo.*

1.2.2.2 Competition (-,-) amenalism (-,0), predation (+,-)

In many cases, interactions result in negative outcomes for organisms within a community. Competition refers to an interaction resulting in both organisms having a negative outcome, amenalism is when one finds a negative outcome while another is unaffected, and predation is when the outcome is positive for one and negative for the other. Collectively, these interactions result in a negative outcome for at least one of the species involved, so I will refer to them as hostile interactions. This term describes the situation when organisms are actively attacking, but the ultimate outcome for the attacker is unclear. Since conflicting interests are common among species competing for the same limited resources, interactions of this nature are thought to be pervasive in microbial communities, and subject to extensive work. I will classify these mechanisms broadly as direct and indirect hostility and provide some examples of their impact in infectious disease. Emphasis will be placed on H_2O_2 and HQNO, mentioned in the previous section, and their implications, as well as those of other mechanisms on microbiogeography.

Direct competition deals with impact of one individual on another not mediated through a third individual or the environment. It can be further divided into contact-dependent and independent mechanisms. Most contact-dependent systems in bacteria have been found to affect host cells rather than bacteria. However, two mechanisms have been studied in the context of microbe-microbe interactions: contact-dependent inhibition (CDI) and type six secretion systems (T6SS)(73). In CDI systems, cells bind to susceptible bacteria and deliver a toxic effector with RNase, DNase, or pore-forming activities, while in T6SS a cellular machinery pierces the cell envelope to deliver the effector proteins(74, 75). Both systems also encode specific immunity proteins that protect the producing cell

from killing. It is worth mentioning that while the systems seem analogous, their activity depends on their spatial structure. CDI has been shown to work in liquid culture, while T6SS has been primarily shown to work on surfaces. This highlights the importance of spatial structure and microbiogeography in microbial communities. Work on T6SS has shown that modulating T6SS activity results in the alteration of spatial patterns formed in a model microbial community(76).

Contact independent mechanisms affect other cells using secreting products. This highlights the key role diffusion plays in delivering the effectors to the target cells and the overall dynamics of interaction. It is in these mechanisms where distances between different organisms can be directly related to the magnitude of interaction between them. Here, I describe two common classes of secreted effectors in bacterial competition: bacteriocins, toxic proteins primarily targeted to closely related organisms; and small molecule antimicrobials

Bacteriocins are one of the earliest discovered players in bacterial hostility(77, 78). They are proteinaceous compounds released by bacteria to attack closely related cells. These proteins typically require binding to a receptor in the target cell. Versions of these proteins are released via contact-dependent hostility, while others are released into the environment. Colicins, one of the first reported bacteriocins, are produced by *E. coli* and possess DNase, RNase or pore-forming activity(79). They are actively transported and release from the cell using a secretion system.

Antimicrobial small molecules kill or slow the growth of a target cell, and unlike contact-dependent mechanisms and bacteriocins, they often affect a broad range of

microbes. Many classes of these molecules that function through a variety of mechanisms are produced by microbes, but emphasis will be placed on HQNO in the *P. aeruginosa*/*S. aureus* interaction and H_2O_2 in the *S. gordonii*/*A. actinomycetemcomitans* interactions, as they are the main actors in work described in the rest of this text.

The *P. aeruginosa* antimicrobial 2-heptyl-4-quinolinol 1-oxide (HQNO) is a potent inhibitor of the respiratory chain in both bacteria and human cells(69). HQNO is produced when P. aeruginosa reaches high cell densities and is further induced during co-culture with *S. aureus* through sensing of extracellular peptidoglycan released by *S. aureus* during normal growth(80). The targeting of the electron transport chain of *S. aureus* during co-culture is associated with *S. aureus* growth inhibition. At sub-MIC levels, HQNO also impacts the physiology of *S. aureus*, promoting resistance to the antibiotic tobramycin(68, 81). The impact of this hostile interaction towards *S. aureus* has been associated with the decreased prevalence of *S. aureus* in individuals with CF as they increase in age(82). *P. aeruginosa* is believed to outcompete *S. aureus* in these chronic infections. However, the capability of a single molecule to promote both synergy and hostility between *P. aeruginosa* and *S. aureus* highlight the complexity of interactions between these organisms and suggests that characterizing their microbiogeography might help us better understand how HQNO impacts spatial structure.

Hydrogen peroxide is a source of reactive oxygen species (ROS), a family of compounds that cause damage to DNA and prevent normal cellular physiology. The oral bacterium *S. gordonii* releases H_2O_2 to toxify its immediate environment and limit access of nutrients to competing species. However, *A. actinomycetemcomitans* produces catalase, which degrades H_2O_2, and ultimately protects it from oxidative stress. The interaction

between these microbes is associated with specific biogeography, where H_2O_2 triggers dispersal of *A. actinomycetemcomitans* to maintain a precise distance from *S, gordonii* that is required for synergy in a mouse abscess model (83) .

Indirect competition refers to an instance when microbes can engage in hostile interactions without a direct attack against other members of the community. One such strategy involves creating an inhospitable environment for other microbes. An example of this mechanism involves acid-producing bacteria. In the context of infectious diseases, S*treptococcus mutans* is known to release lactic acid as by-product of fermentation, which lowers the pH of the environment and restricts the area to acid-tolerant organisms. This interaction and its impact on microbiogeography are further explored in Chapter 2.

Another instance of indirect competition involves nutrient acquisition. In this case, a microbe can withhold nutrients from other microbes to prevent their growth. One example is the use of siderophores—molecules that bind and transport iron—to sequester iron from the environment, limiting availability for neighboring microbes(84, 85). While siderophores are released in the environment, specific binding motifs restrict their import to certain microbes. The dynamics of siderophore import has been studied in the context of viscosity and spatial structure of the community, showing that higher viscosity increases the efficiency of mechanisms maintaining the target specificity(86). These mechanisms show the environment also plays a role in interactions within microbial communities.

1.2.3 The impact of spatial structure in microbial communities

The outcomes of interactions between microbes depends on several factors. In controlled environments, like in a laboratory setting, the outcome is typically dictated by

the organisms and their metabolic capabilities. However, it is essential to recognize the role of the environment in interactions within microbial communities. There are two specific requirements that need to be met in the study of microbial interactions in the context of infectious diseases under laboratory conditions: 1) use interacting bacteria that have been shown to be found together in the community of interest; 2) use a lab environment that mimics the infection site. Below, I discuss studies that satisfy these requirements and have provided mechanistic insights into the emergence of microbiogeography.

1.2.3.1 *P. aeruginosa* in high viscosity in vitro systems

As mentioned before, viscosity plays a key role in microbial interactions as it dictates diffusion rates of secreted molecules. Consequently, several studies have characterized microbial interactions in varying degrees of viscosity. In the context of infectious diseases, increasing viscosity of aqueous media more closely resembles the environment of infections. This approach can help identify some differences between model systems and the infection site on infection dynamics and microbial interactions.

Elaborating on previously described systems, one study observed populations of *P. aeruginosa* and siderophore production in the context of hostile interactions within species. Specifically, by some individuals capitalizing on gains generated by other members of the population without incurring the cost, a phenomenon known as cheating(87). Increasing the relative abundance of cheaters typically results in a population decline, as not enough resources are being produced to sustain high levels of cheaters. This study showed increasing the viscosity led to decreased abundance of cheaters via a combination of limited dispersal of cells and limited diffusion of siderophores(88). Other studies have also shown

the impact of spatial structure in modulating cheating behavior(89) .This effect might be responsible for monitoring cheaters in environments with high viscosity, like infection of the cystic fibrosis lung.

Interactions between *P. aeruginosa* and *S. aureus* have also been studied at different degrees of viscosity and has shown that the fitness of one or both species can be affected by it(90). In Chapter 2, the interactions between these organisms are explored in synthetic cystic fibrosis media (SCFM2), a viscous environment that mimics the nutritional and physical properties of sputum from individuals with CF.

1.2.3.2 Oral microbiota

The oral cavity has several characteristics that have facilitated laboratory study of interactions between microbes in the cavity since the earliest days of microbiology. These characteristics include hosting hundreds of different species, being able to form several microenvironments with different physical and nutritional properties, and its ease for direct sampling. Consequently, some of the dynamics of oral communities, particularly their assembly, are well-characterized(91).

Early observations led to the conclusion that the initial community in the mouth is composed of cocci, primarily *Streptococcus* and *Actinomyces(92)*. These species can bind directly to a coat of saliva at the surface of epithelial cells and form a scaffold where other bacteria can assemble. Recent observations using fluorescent labeling of oral organisms found that filamentous bacteria, including *Cornybacterium*, stem out from the scaffold and are "decorated" with other forms of cocci, forming the corncob structure described earlier(54). This observation contrasts previous hypotheses that argued *Fusobacterium*

nucleatum played a key role on the assembly and structure of the oral community since it was found to coaggregate with several other oral species(93). This story highlights the value of combining highly controlled laboratory experiments with the direct sampling of infections and how they can lead to new insights.

The work described in later chapters expands on the work explained above and aims to address basic questions about the impact of microbial structure in microbial communities using several model communities in infection and infection-like systems. The decision to use communities as a model, instead of individual microbes, is to emphasize the polymicrobial nature of disease and understanding it thoroughly. Moreover, it has been mentioned before that "There is no single natural scale at which ecological phenomena should be studied."(20)

1.3 Addressing Unanswered Questions in Microbiogeography

Having established how specific patterns of biogeography can help us understand the dynamics of a system, what are the basic mechanisms bacteria use to interact and the impact that biogeography has on microbial interactions? Previous publications and the following chapters describe work addressing questions regarding the spatial structure and its impact on microbial communities. Kim et al(55) describes previous analyses of microbial communities and a framework I developed to quantitatively characterize microbiogeography using confocal images of *in vitro* systems and human infections and finds a specific spatial structure is required for infection. This framework includes the identification of elements described in this chapter, including proportional occupancy. Chapter 2 incorporates genetic tools and addresses the question: How does manipulation

of known microbial interactions impact on spatial structure? For this question, the interactions between *P. aeruginosa* and *S. aureus* are characterized in SCFM2, and the impact of the molecule HQNO is examined. The next chapters expand on that work by manipulating interaction in two different animal infection models. In chapter 3 I use the *P. aeruginosa* and *S. aureus* model community in chronic wounds and modulate their hostile interactions via phenazine and HQNO production. In Chapter 4 I use *S. gordonii* and *A. actinomycetemcomitans* in a mouse thigh abscess model and modulate their cross-feeding and cross-respiration interactions involving hydrogen peroxide and lactate. Throughout this work, I quantitatively characterize the *microbiogeography* of bacteria in infection and infection-like environments to identify mechanisms that can help predict disease dynamics.

CHAPTER 2. A *P. AERUGINOSA* ANTIMICROBIAL AFFECTS THE BIOGEOGRAPHY BUT NOT FITNESS OF *S. AUREUS* DURING CO-CULTURE

2.1 Introduction

Polymicrobial infections often cause more damage and are more recalcitrant to clearance than those caused by a single microbe (5, 6, 65, 94, 95). Two bacteria commonly found together in human polymicrobial infections are *Pseudomonas aeruginosa* and *Staphylococcus aureus*, which cause chronic infections at a number of body sites in individuals with a variety of comorbidities including cystic fibrosis (CF) (96, 97). *P. aeruginosa* and *S. aureus* are the two most common bacteria infecting the CF lung, and their co-infection is associated with increased morbidity and mortality (98-101). Experiments in animal models co-inoculated with *P. aeruginosa* and *S. aureus* indicate that co-infection increases disease severity and antimicrobial resistance (80, 102-105).

While animal models have provided insights into *P. aeruginosa-S. aureus* co-infections, in many cases the molecular mechanisms controlling enhanced pathogenesis and antimicrobial resistance are not known. One of the challenges to defining co-infection mechanisms is that animal models of infections are constrained in model design, both in regard to the numbers of bacteria required for establishing an infection and duration of the

---

*This chapter was adapted from the following reference: Barraza, Juan P., and Marvin Whiteley. "A *Pseudomonas aeruginosa* antimicrobial affects the biogeography but not fitness of *Staphylococcus aureus* during coculture." *mBio* 12.2 (2021): e00047-21. Reused with permission. I was the primary author of this work.

infection. In addition, time-resolved, simultaneous assessment of bacterial fitness, spatial structure, and function is often not feasible in animal models. This has necessitated the development of versatile, *in vitro* models to discover and molecularly characterize *P. aeruginosa*-*S. aureus* co-culture interaction mechanisms, which can subsequently be studied in animal models. However, developing *in vitro* experimental models has been challenging as *P. aeruginosa* is highly lytic for *S. aureus* under most *in vitro* co-culture conditions (59, 104-111). As a consequence, co-cultures are generally only stable when *P. aeruginosa* is at low cell density (110). Given these challenges, work to mechanistically characterize interactions between *P. aeruginosa* and *S. aureus* has often been performed by exposing one bacterium to the cell-free supernatant of the other (68, 112-114). These studies have shown *P. aeruginosa* anti-staphylococcal activity is driven by exoproducts including proteases and secondary metabolites such as hydrogen cyanide, phenazines, and quinoline *N*-oxides (69, 106, 115-117).

One of the most widely recognized exoproducts of *P. aeruginosa* with potent anti-staphylococcal activity is 2-heptyl-4-hydroxyquinoline N-oxide (HQNO). HQNO has been found in CF lung exudates and kills *S. aureus* by inhibiting cellular respiration and reducing cellular ATP (69, 81, 118). In addition to its potent anti-staphylococcal activity, sub-lytic levels of HQNO can alter the physiology of *S. aureus* by shifting its metabolism from respiration to fermentation (119), increasing biofilm formation (114), inducing a small-colony variant phenotype (120), and increasing its susceptibility to membrane-targeting antimicrobials, (113) while decreasing its susceptibility to aminoglycosides (112).

While supernatant addition experiments have identified HQNO and other potential interaction mechanisms driven by secreted products, they do not allow for study of cell-

cell interactions or the spatial organization of the microbial community, both of which impact polymicrobial infection outcomes (1, 55, 83, 121, 122). Thus, there is a need for experimental models that allow for stable co-culture of *P. aeruginosa* and *S. aureus* in the laboratory. Several studies have developed such systems by altering the bacterial genotype or growth conditions. For example, *in vitro* co-existence has been obtained by using a mucoid strain of *P. aeruginosa* that has less lytic activity against *S. aureus* (123), exchanging media and removing planktonic cells to extend co-existence (119), or by altering the frequency of *P. aeruginosa*/*S. aureus* or the growth environment (90, 108). However, laboratory co-culture models can be further improved with the explicit goal of mimicking both the chemical and physical environment of the human infection site (6, 124).

In this study, we combine ecological and molecular techniques to understand interactions between *P. aeruginosa* and *S. aureus* in an *in vitro* infection model (Synthetic CF sputum Media, SCFM2) that has been shown to mimic the chemical and physical environment of expectorated CF sputum (59, 61, 109, 125, 126). We demonstrate that *S. aureus* and *P. aeruginosa* robustly co-exist in SCFM2 under static, but not mixed co-culture. Then, using high resolution confocal microscopy and a computational framework that quantifies spatial structure at the micron-scale, we find that HQNO can alter spatial patterning between the two species without altering fitness. Further, we show that HQNO increases tolerance of *S. aureus* to the aminoglycoside tobramycin in co-culture with *P. aeruginosa*.

2.2 Results and Discussion

2.2.1 *P. aeruginosa* and *S. aureus* co-exist in static but not well-mixed SCFM2.

The goal of this study was to develop a biologically relevant *in vitro* experimental system that allows for co-existence of *P. aeruginosa* and *S. aureus* and provides the versatility to study their interactions with micron-scale spatial resolution. The system we chose was co-culture in SCFM2, a defined media designed by quantifying the chemical composition of sputum expectorated by individuals with CF (126). The gene expression signature of *P. aeruginosa* grown in SCFM2 is more similar to CF sputum directly harvested from humans than other CF pre-clinical models, including a mouse acute lung model (125). *P. aeruginosa* also requires similar genes to grow in SCFM2 as it does *ex vivo* in expectorated human CF sputum (126). Importantly for this study, SCFM2 contains relevant levels of DNA and mucin, which promotes the natural formation of *P. aeruginosa* aggregates with sizes similar to those observed in the CF lung (59, 61). SCFM2 has also been shown to be a valuable model for studying *S. aureus* CF infection including understanding how host immune components affect *S. aureus* physiology and gene expression (99, 124). Of note, growth of both *P. aeruginosa* and *S. aureus* in SCFM2 has been performed previously without mixing under static growth conditions (59, 61, 124, 126).

To determine whether these bacteria can stably co-exist in SCFM2, laboratory strains of *P. aeruginosa* (PA14) and *S. aureus (*LAC) were co-inoculated into SCFM2 at a 1:1 frequency, cultures were incubated statically or mixed with a magnetic stir bar, and bacterial numbers were quantified at 4-hour intervals using agar plate counts on selective media. These strains are well-characterized laboratory strains, highly virulent and antagonistic, have been used to study *P. aeruginosa-S. aureus* interactions (102, 123, 127,

128), and are representative of other pathogenic strains of the same species, thus incorporating clinical relevance to the study. In addition, these strains display gene expression patterns and aggregate sizes in SCFM2 that are similar to that in human expectorated CF sputum (59, 61, 124, 125, 129). As these are not highly adapted CF strains, they serve as a model to study potential interactions in early CF disease. There is no doubt that using adapted CF strains would be more relevant. However, our recent studies show that gene expression of CF-adapted strains in SCFM2 are only slightly more representative of that in later CF disease than lab strains (125). Thus, our studies will likely have some relevance for understanding later stage disease.

Our results reveal that, as previously observed, *P. aeruginosa* is highly lytic for *S. aureus* in well-mixed co-cultures, reducing *S. aureus* numbers by ~10,000-fold between hours 8 and 12 (Fig. 1A). However, this decrease in *S. aureus* numbers was not observed when co-cultures were incubated statically (Fig. 1B). Moreover, both *P. aeruginosa* and *S. aureus* grew to a similar density in static co-culture as they did in static mono-culture (Fig. 1, red lines). These results indicate that *P. aeruginosa* and *S. aureus* co-exist in SCFM2 when grown under static conditions with no loss of fitness compared to mono-culture static growth.

2.2.2 Anti-staphylococcal activity in *P. aeruginosa* is higher in well-mixed culture conditions.

P. aeruginosa produces several secreted anti-staphylococcal molecules, and many of these molecules are produced at higher levels in the presence of oxygen (130, 131). Thus, we hypothesized that a primary mechanism promoting stable *P. aeruginosa*-*S. aureus*

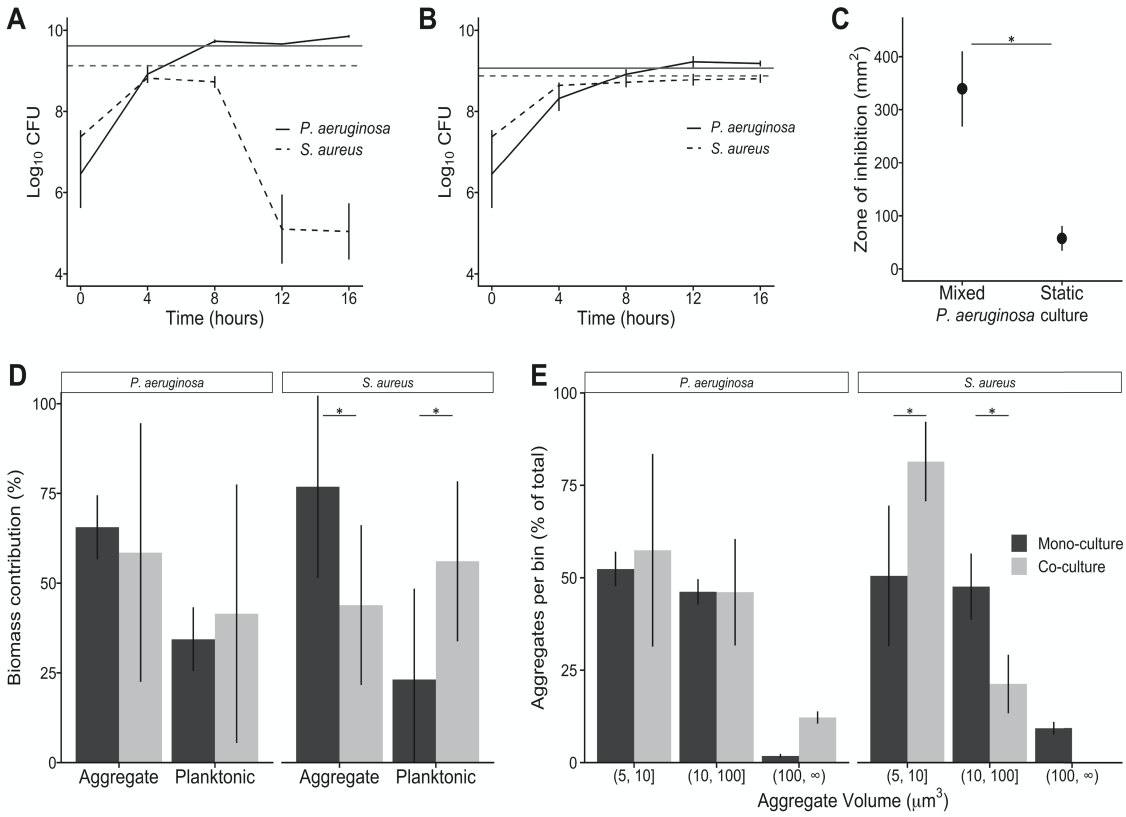

Figure 2-1 *S. aureus* and *P. aeruginosa* stably co-exist in static SCFM2.

Growth of *P. aeruginosa* PA14 and *S. aureus* LAC under (A) well-mixed and (B) static conditions in SCFM2 (n=3). Black lines represent colony forming units (CFUs) in co-culture, and the red lines indicate growth yield after 16 hours in mono-culture. (C) Zone of inhibition produced by *P. aeruginosa* supernatants spotted on filter discs on lawns of *S. aureus*. *P. aeruginosa* produced a larger zone of inhibition when grown well-mixed in SCFM2 compared to static SCFM2 (n=5, paired Student's t-test, $P = 1 \times 10^{-3}$). (D) Aggregate and planktonic biomass of *P. aeruginosa* and *S. aureus* in SCFM2 in mono- and co-culture. *S. aureus* biomass primarily exists as aggregates in mono-culture and as planktonic cells in co-culture. The black line is mono-culture and gray is co-culture (n=3, paired Student's t-test, $P = .02$ for both comparisons). (E) Number of aggregates of *P. aeruginosa* and *S. aureus* within different aggregate size ranges in mono- and co-culture. We quantified the number of aggregates in three size ranges: 5 μm^3 to 10 μm^3, 10 μm^3 to 100 μm^3, and larger than 100 μm^3 and reported the percentage of total aggregates in each size range. A lower percentage of aggregates were observed in the 5 – 10 μm^3 range during mono-culture compared to co-culture (50% vs 80%) for *S. aureus* (n=3, paired Student's t-test, $P = .05$), and a correspondingly higher percentage of aggregates in the 10 – 100 μm^3 range were observed in co-culture compared to mono-culture (20% vs 47%) (paired Student's t-test, $P = .03$). The black line is mono-culture and gray is co-culture. Error bars are standard deviation. (* indicates $P < .05$ by paired Student's t-test.)

co-culture in static conditions was decreased production of anti-staphylococcal molecules by *P. aeruginosa* due to decreased mixing. To test this hypothesis, cell-free supernatants from *P. aeruginosa* grown in SCFM2 under mixed and static conditions were collected and assessed for the ability to inhibit *S. aureus* growth using a disc diffusion assay (Fig. 1C). For this assay, *P. aeruginosa* supernatant was added to a filter disc on an agar plate containing *S. aureus* and the zone of inhibition was measured. *P. aeruginosa* grown well-mixed in SCFM2 produced a zone of inhibition with a diameter more than ~6 times larger than growth in static culture (Fig. 1C). These results reveal that *P. aeruginosa* supernatants from well-mixed cultures possess higher anti-staphylococcal activity than those from static cultures.

Our findings that ecological factors (well-mixed and static growth) affect *P. aeruginosa* anti-staphylococcal activity and the outcome of *P. aeruginosa*-*S. aureus* co-culture dynamics are fundamentally in agreement with recent work from Niggli et al. (108), which showed that *P. aeruginosa* and *S. aureus* co-exist in a laboratory medium that promotes aggregation by embedding in low levels of agar. However, this study did not observe an increase in *P. aeruginosa* relative fitness compared to *S. aureus* during growth in mixed conditions compared to agar conditions, which differs from our observations (Fig. 1A&B). The reason for this is not clear, but is likely explained by low aeration of the mixed culture condition used in the Niggli study (108). This study performed mixed co-culture in laboratory medium in wells of 24 well plates, using a volume of 1.5 ml in a well with a maximum volume of 3.4 ml and shaking at 170 rpm (108). In our experience, *P. aeruginosa* requires high shaking rates (250 rpm) and low culture volume/culture vessel volume (1/10 to 1/50) for sufficient aeration, and these culture conditions lead to high anti-staphylococcal

activity (104, 107, 109, 110). Here, we mixed SCFM2 using a stir bar at 250 rpm to ensure high levels of aeration. Regardless, both studies agree that *P. aeruginosa* and *S. aureus* co-exist in culture conditions that promote aggregation, which restricts movement and promotes the development of spatial structure.

2.2.3 Aggregate sizes and distributions in *P. aeruginosa*-*S. aureus* mono- and co-cultures.

The micron-scale spatial structure of infecting polymicrobial communities has been shown to affect infection severity in a mouse abscess model (83); thus, one of the goals of this work was to develop a biologically relevant experimental system that allows for the spatial structure of *P. aeruginosa* and *S. aureus* to be assessed temporally and at the micron-scale. Based on the diversity of interactions that have been described, we hypothesized that there would be significant differences in spatial structure of *P. aeruginosa*-*S. aureus* co-cultures compared to mono-culture, despite the fact that cell numbers are equivalent (Fig. 1B). To test this hypothesis, we inoculated *P. aeruginosa* expressing the green fluorescent protein (GFP) and *S. aureus* expressing the red fluorescent protein DsRed in mono- and co-culture (1:1 frequency) into SCFM2, incubated them statically, and imaged them using confocal laser scanning microscopy (CLSM) (Fig 2-2). We chose to end our experiments at 5 hours for several reasons: 1) transcriptomic analysis of *P. aeruginosa* at the 5-6 hour timepoint in SCFM2 has been shown to most accurately mimic the gene expression of *P. aeruginosa* in human expectorated sputum (125, 129); 2) transcriptomic analysis of *S. aureus* in SCFM2 at this timepoint is also similar to that in human expectorated sputum (124); 3) *P. aeruginosa* naturally forms aggregates in SCFM2 with similar size to those in expectorated CF sputum at this timepoint (59); 4) *S. aureus*

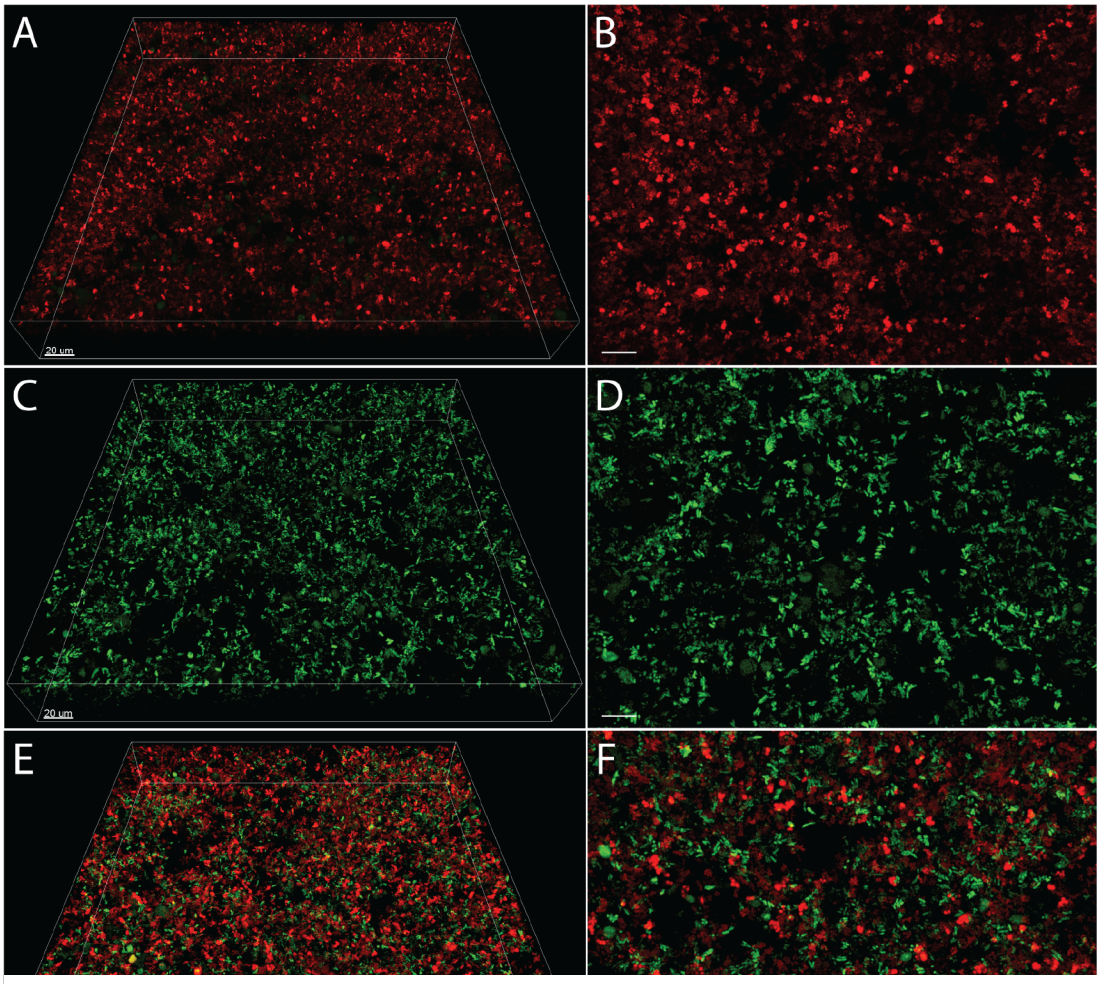

Figure 2-2 Images of *P. aeruginosa* and *S. aureus* co-culture in SCFM2.

Images of *P. aeruginosa* and *S. aureus* in mono- and coculture in SCFM2. Representative confocal images of DsRed-expressing *S. aureus* LAC (red) in (A and B) monoculture, GFP-expressing *P. aeruginosa* PA14 (green) in monoculture (C and D), and *S. aureus* and *P. aeruginosa* in coculture (E and F). Images on the left (A, C, and E) show the entire imaging field of 270 µm by 270 µm by 40 µm. Images on the right (B, D, and F) show a close-up view of images on the left. Bars, 10 µm unless otherwise noted.

and *P. aeruginosa* numbers at this timepoint are within the range often observed in human CF sputum; and 5) *S. aureus* has just reached maximum growth yields at this timepoint, and DsRed fluorescence fades rapidly as the cells progress deeper into stationary phase.

To quantify the spatial structure of each culture, we utilized a custom computational pipeline (publicly available at https://jupabago.github.io/PaSaProject/) that was recently used to quantify the spatial structure of bacterial communities on human teeth (55). The first step in this pipeline is to discriminate between bacterial cells growing planktonically and those growing as aggregates (biofilms). To accomplish this, we first identified all bacterial objects from CLSM images and classified them by volume, using previously established guidelines defining planktonic cells as objects <5 μm^3 and aggregates as ≥5 μm^3 (59). This analysis revealed that *S. aureus* and *P. aeruginosa* are present as both planktonic cells and aggregates in mono- and co-culture in SCFM2 (Fig. 2-1D). However, the percentage of *S. aureus* biomass in aggregates in mono-culture (~75%), was twice as high as in co-culture, and correspondingly planktonic cells contributed less to the total biomass in mono- compared to co-culture (Fig. 2-1D). In contrast, aggregates of *P. aeruginosa* in mono and co-culture contributed equally to total biomass, although the co-culture values displayed higher variance (Fig. 2-1D).

Next, we focused only on the portion of the biomass in aggregates to ask if co-culture impacted aggregate size. We defined bins of increasing aggregate size and quantified the number of *P. aeruginosa* and *S. aureus* aggregates within each bin (Fig. 2-1E). The bin sizes were chosen to include the most common observed aggregate size range in human expectorated sputum (10-100 μm^3) as well as a smaller and a larger bin (59, 132-134). *P. aeruginosa* aggregate size was not affected by the presence of *S. aureus* with over 95% of

aggregates ≤100 μm^3 in both mono- and co-culture. However, *S. aureus* had a higher percentage of aggregates that were ≤10 μm^3 in co-culture compared to mono-culture (80% vs 50% respectively) and a correspondingly lower percentage that were between 10-100 μm^3 (20% vs 47%).

Collectively, these results reveal that while *P. aeruginosa* and *S. aureus* both exist as aggregates and planktonic cells in mono- and co-culture, the *S. aureus* population shifts towards planktonic cells and small aggregates during co-culture. The biological relevance of the shift of *S. aureus* to a more planktonic mode during co-culture is not known. However, as there is no decrease in fitness in co-culture compared to mono-culture under static growth conditions (Fig. 1B), it is clear that it is not necessary for *S. aureus* to grow as large aggregate biofilms to be fit in the presence of *P. aeruginosa*. The finding that *P. aeruginosa* exists as both aggregate (65% biomass in mono-culture, Fig. 1D) and planktonic cells (35% biomass in mono-culture, Fig. 1D) in SCFM2 further supports the biological relevance of this model, as recent studies reveal that *P. aeruginosa* exists in expectorated CF sputum as both aggregate (~75% of biomass) and planktonic (~25% of biomass) cells (59, 132, 134).

2.2.4 Impact of HQNO on *P. aeruginosa*-*S. aureus* community structure

As we have now developed a biologically relevant co-culture model for studying *P. aeruginosa*-*S. aureus* interactions, we next sought to examine the impact of *P. aeruginosa*-produced HQNO on this community. We chose HQNO as it not only has antimicrobial activity against *S. aureus*, but sub-inhibitory levels impact the physiology of *S. aureus*, including susceptibility to antimicrobials (112-114, 119, 120). In addition, the gene

encoding the enzyme required for the final step in HQNO biosynthesis (*pqsL*) is expressed similarly in static SCFM2 at the 5-hour time point and in human expectorated sputum (125), providing evidence of the biological relevance of SCFM2 for studying HQNO at this timepoint.

To examine the role of HQNO on community structure, we first created a strain of *P. aeruginosa* that does not produce HQNO by deleting *pqsL* (*P. aeruginosa ΔpqsL*) and showed that complementation of this strain with *pqsL in trans* restored *S. aureus* lytic ability (Appendix Fig S-1) Next, we co-cultured *S. aureus* under mixed and static conditions with *P. aeruginosa ΔpqsL*. Under well-mixed conditions, *P. aeruginosa ΔpqsL* lysed *S. aureus*, but to a lesser degree than wild-type *P. aeruginosa*, reducing *S. aureus* numbers by ~100 fold between 8 and 12 hours (Fig. 2-3A). Under static growth conditions, *P. aeruginosa ΔpqsL* and *S. aureus* co-existed and reached similar growth yields in both mono- and co-culture (Fig. 2-3B). As expected from the decrease in *S. aureus* levels at late stages of growth, supernatants from *P. aeruginosa ΔpqsL* grown well-mixed exhibited anti-staphylococcal activity against *S. aureus* using the disc diffusion assay (Fig. 2-3C). This activity was less than that observed for well-mixed wild-type *P. aeruginosa* ($P = .023$, Student's t-test) and similar to that observed for supernatants from static wild-type *P. aeruginosa*. However, supernatants from *P. aeruginosa ΔpqsL* grown statically had little antimicrobial activity (Fig. 2-3C). These data reveal that the anti-staphylococcal activity of HQNO has biological importance in well-mixed, but not static, co-culture conditions, and that HQNO is not the only lytic factor in well-mixed SCFM2 co-cultures.

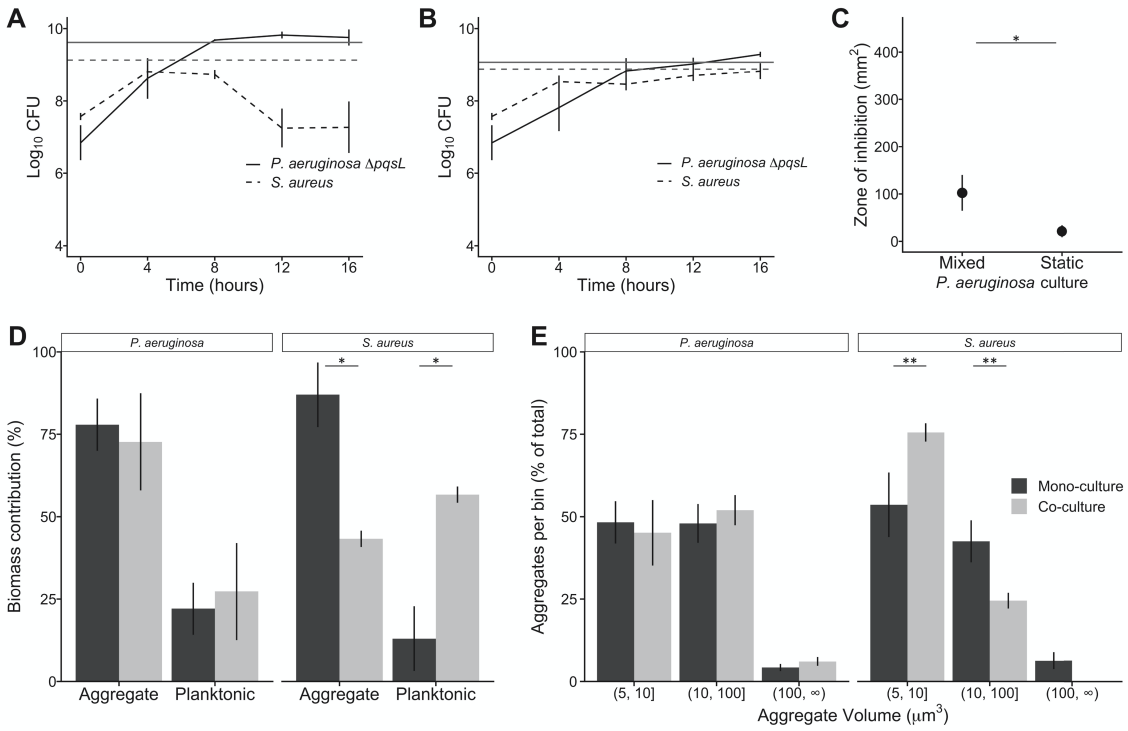

Figure 2-3 HQNO impacts *S. aureus* fitness in well-mixed but not static SCFM2 co-cultures.

Growth of *P. aeruginosa ΔpqsL* and *S. aureus* under (A) well-mixed and (B) static conditions in SCFM2 (n=3). Black lines represent colony forming units (CFUs) over time in co-culture, and the red line indicates growth yield after 16 hours in monoculture. (C) Zone of inhibition produced by *P. aeruginosa ΔpqsL* supernatants spotted on filter discs on lawns of *S. aureus*. *P. aeruginosa* produced a larger zone of inhibition when grown well-mixed in SCFM2 compared to static SCFM2 (n=5, paired Student's t-test, $P = .012$) but not as large as wild-type *P. aeruginosa* ($P = .023$, Fig. 1C). (D) Aggregate and planktonic biomass of *P. aeruginosa ΔpqsL* and *S. aureus* in SCFM2 mono- and co-culture. Similar to co-culture with wild-type *P. aeruginosa*, *S. aureus* biomass primarily exists as aggregates in mono-culture and as planktonic cells in co-culture (paired Student's t-test, $P = .02$). *P. aeruginosa ΔpqsL* mono-culture biomass was also found to be more present as aggregates than as planktonic cells (paired Student's t-test, $P = .02$). (E) Number of aggregates of *P. aeruginosa ΔpqsL* and *S. aureus* within different aggregate size ranges in mono- and co-culture. We quantified the number of aggregates in three size ranges: 5 μm^3 to 10 μm^3, 10 μm^3 to 100 μm^3 and larger than 100 μm^3, and reported the percentage of total aggregates in each size range. Fewer aggregates were observed in the 5 – 10 μm^3 range during mono-culture compared to co-culture for *S. aureus* (n=3, paired Student's t-test, $P = .08$) and a corresponding higher percentage of aggregates in the 10 – 100 μm^3 range were observed in the mono-culture compared to co-culture (n=3, paired Student's t-test, $P = .08$). Error bars are standard deviation. (* indicates $P < .05$ and ** indicates $P < .1$ by paired Student's t-test).

2.2.5 Aggregate sizes and distributions in *P. aeruginosa ΔpqsL* and *S. aureus* mono- and co-cultures

While HQNO had no effect on *S. aureus* fitness during static co-culture, we next assessed whether this molecule impacted *P. aeruginosa ΔpqsL* and *S. aureus* aggregate number and size using confocal microscopy (Fig. 2-4), as described above for wild-type *P. aeruginosa*-*S. aureus* co-cultures (Fig. 2-1D-E). This analysis revealed that co-cultures containing *P. aeruginosa ΔpqsL* (Fig. 2-3D) were overall similar to those with wild-type *P. aeruginosa* (Fig. 2-1D) in regard to aggregate biomass, with *P. aeruginosa ΔpqsL* primarily found as aggregates in both mono (77%) and co-culture (72%), and *S. aureus* existing primarily as aggregates in mono-culture and as planktonic cells in co-culture (Fig. 2-3D). Similar to wild-type *P. aeruginosa*, *P. aeruginosa ΔpqsL* aggregate size was not affected by the presence of *S. aureus* with over 95% of aggregates ≤100 μm^3 in both mono- and co-culture (Fig. 2-3E). In addition, *S. aureus* had a higher percentage of aggregates that were ≤10 μm^3 in co-culture compared to mono-culture (75% vs 55%, respectively) and a correspondingly lower percentage that were between 10-100 μm^3 (25% vs 40% respectively). These results reveal that although HQNO is an important contributor to *S. aureus* lysis during well-mixed co-culture, it plays no role in *P. aeruginosa* and *S. aureus* aggregate biomass and size during static co-culture.

2.2.6 HQNO impacts spatial organization of *P. aeruginosa* and *S. aureus* co-cultures.

While HQNO had no detectable effect on biomass or aggregate size during co-culture, we hypothesized that due to its antimicrobial activity, this molecule would impact the spatial organization of the community by increasing the distance between *P. aeruginosa*

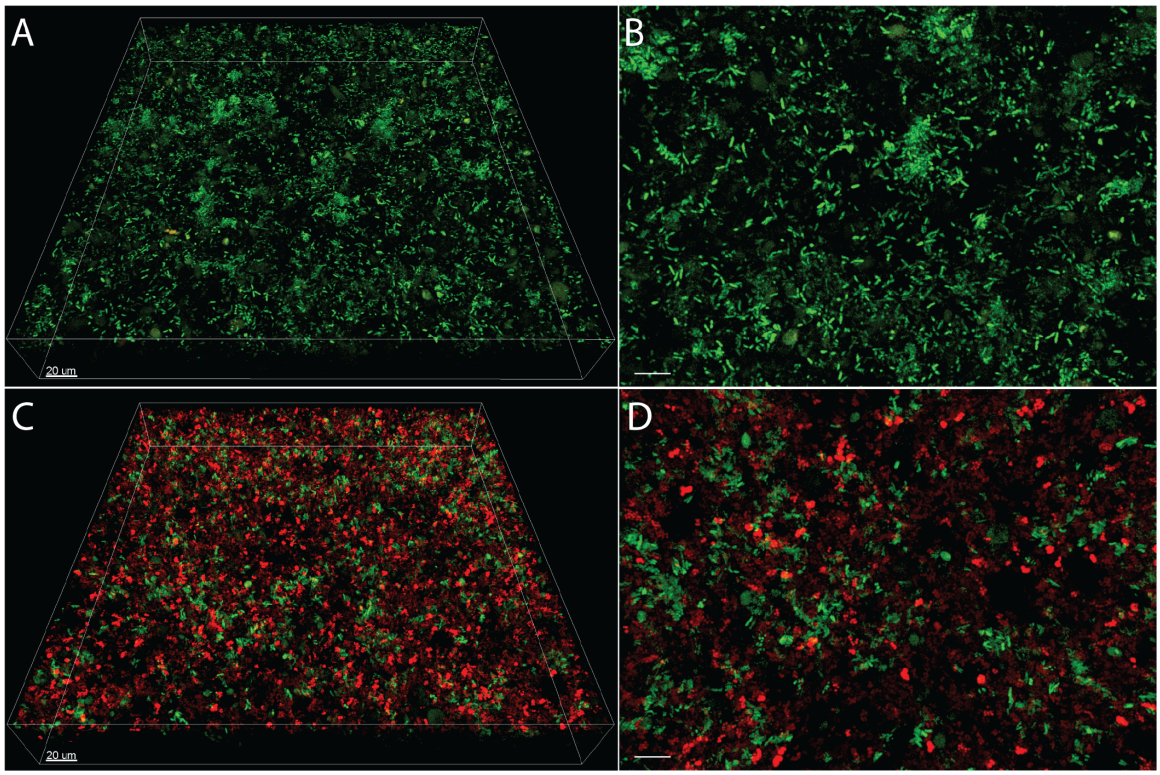

Figure 2-4 Images of *P. aeruginosa* Δ*pqsL* in mono- and coculture with *S. aureus* in SCFM2.

Representative confocal images of GFP-expressing *P. aeruginosa* Δ*pqsL* PA14 (green) in (A and B) monoculture and (C and D) coculture with DsRed-expressing *S. aureus* LAC (red). Images on the left (A and C) show the entire imaging field of 270 µm by 270 µm by 40 µm. Images on the right (B and D) show a close-up view of images on the left. Bars, 10 µm unless otherwise noted.

and *S. aureus*. To test this hypothesis, we quantified spatial organization of *P. aeruginosa-S. aureus* co-cultures using two metrics: co-aggregation and enrichment distance.

Co-aggregation is a common occurrence in many microbial systems and can be quantified by counting the prevalence of aggregates that contain multiple species (135). To test for co-aggregation in the *P. aeruginosa-S. aureus* SCFM2 static co-cultures, we quantified the proportion of aggregates that contain both *P. aeruginosa and S. aureus*. Our results reveal that co-aggregation does not comprise a significant portion of the total biomass in co-cultures containing either wild-type *P. aeruginosa* or *P. aeruginosa ΔpqsL*, with 1-3% of the total aggregates containing both *P. aeruginosa* and *S. aureus* (Fig. 2-5A). These data indicate that wild-type *P. aeruginosa* and *S. aureus* do not produce substantial numbers of mixed species aggregates in SCFM2, and the elimination of HQNO does not impact the prevalence of mixed aggregates. These data are also consistent with previous data examining co-aggregation of *P. aeruginosa* PA14 strains that express different fluorescent proteins, which revealed that *P. aeruginosa* aggregates primarily arise from single cells (61).

We next asked whether *P. aeruginosa* and *S. aureus* were randomly distributed in SCFM2 or if there was spatial patterning. To answer this question, we characterized spatial patterning of *P. aeruginosa-S. aureus* aggregates by calculating enrichment distance. To determine this metric, we first calculated proportional occupancy, which quantifies the composition of the immediate surroundings of a focal community member in relation to other community members at various distance intervals in three dimensions at the micron scale (55). Then, enrichment distance was defined as the distance from the focal species at which the proportional occupancy of the target species is the highest. Thus, enrichment

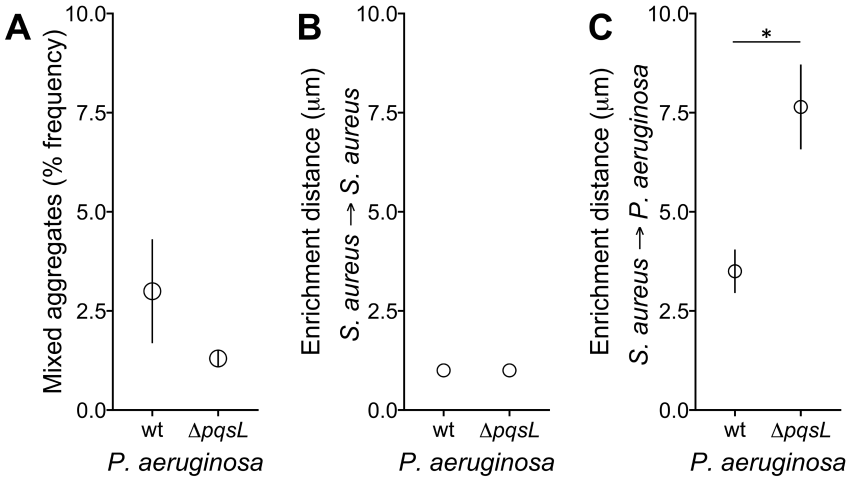

Figure 2-5 HQNO impacts the spatial organization of P. aeruginosa and S. aureus communities.

(A) Percent mixed-species aggregates of S. aureus with P. aeruginosa wild-type (wt) and Δ*pqsL* during static growth in SCFM2. (B) Enrichment distance calculated using S. aureus as both the focal species and target species, indicating that S. aureus is most often found tightly associated with other S. aureus cells. (C) Enrichment distance calculated using S. aureus as the focal species and P. aeruginosa as the target species. S. aureus was localized closer to wild-type P. aeruginosa than P. aeruginosa Δ*pqsL* (paired Student's *t* test, $P = 0.01$). Error bars show standard deviations

distance indicates where biomass of the target species is over-represented in relation to the focal species. We calculated enrichment distance for co-cultures using *S. aureus* as the focal species and *S. aureus* or *P. aeruginosa* as the target species, for both wild-type *P. aeruginosa* and *P. aeruginosa ΔpqsL*. In each case, we chose five thousand random DsRed voxels corresponding to *S. aureus* for each replicate and calculated the prevalence of target species voxels within defined distance intervals (30 intervals, each 1 μm in size). Our results reveal that the enrichment distance of *S. aureus* to *S. aureus* was 0-1 μm when co-cultured with either wild-type or *ΔpqsL* (Fig. 2-5B), which is the smallest distance interval tested. These results indicate that on average, an *S. aureus* cell is most often located within 1 μm from a second *S. aureus* cell. These results make intuitive sense and serve as a control for our metric, as a proportion of *S. aureus* in these communities exists in aggregates, which are by definition tightly associated groups of cells. The enrichment distance of *S. aureus* to wild-type *P. aeruginosa* was 3.5 μm, indicating that during static co-culture in SCFM2 these two bacteria exist in close proximity to one another (Fig. 2-5C). Intriguingly, *S. aureus* was on average found at a further distance from *P. aeruginosa ΔpqsL* (7.6 μm) than from wild-type *P. aeruginosa*. Thus, although HQNO does not impact the fitness *S. aureus* and *P. aeruginosa* (Figs. 2-1 and 2-3), it does affect the spatial structure of the community.

These latter results are surprising as we expected that elimination of a potent antimicrobial would allow for closer association between *P. aeruginosa* and *S. aureus*. While the mechanism(s) underlying this phenotype are not known, one simple model is competition for molecular oxygen as an electron acceptor. *P. aeruginosa* predominantly respires to generate energy, and while there are low levels of nitrate in SCFM2 that can be used (350 μM), significantly higher levels (50 mM) are needed to support high yield growth

of *P. aeruginosa* in SCFM (136). Thus, O_2 is likely the predominant electron acceptor used during growth in SCFM2. HQNO has been shown to shift *S. aureus* metabolism from respiration to fermentation (119), which may allow for close co-localization by preventing competition for O_2. Elimination of HQNO would likely cause competition for O_2, which would lead to *P. aeruginosa* growing in locations where O_2 levels are higher, further from *S. aureus*. Testing this model will require, amongst other approaches, a technological advancement in micron-scale oxygen measurement, which we are currently pursuing using electrochemical approaches.

2.2.7 HQNO enhances tobramycin resistance in *S. aureus* during co-culture, although mono-cultures of *S. aureus* are still more resistant.

Previous studies have shown that the presence of HQNO in *P. aeruginosa* supernatants enhances aminoglycoside resistance in *S. aureus* (68). Thus, we used our system to assess whether these findings are also observed in co-cultures. We incubated *S. aureus* statically in mono- or co-culture with *P. aeruginosa* in SCFM2 for three hours, then treated with a level of tobramycin (256 μg/ml) that results in 90% killing of mono-culture *S. aureus* grown static in SCFM2 (Fig. 2-6). Co-culture with either wild-type *P. aeruginosa* or *ΔpqsL* increased *S. aureus* susceptibility to tobramycin compared to mono-culture (Fig. 2-6). Further, this increased susceptibility was greatest in co-culture with the *ΔpqsL* mutant, which showed a 10-fold decrease in *S. aureus* numbers relative to co-culture with wild-type *P. aeruginosa*. These results reveal that similar to previous experiments with *P. aeruginosa* supernatants, HQNO enhances tobramycin resistance of *S. aureus* during co-culture with *P. aeruginosa*. However, *S. aureus* mono-cultures are significantly more resistant to tobramycin killing than co-cultures with *P. aeruginosa*, suggesting that

ultimately *P. aeruginosa* is sensitizing *S. aureus* to tobramycin killing even in the presence of HQNO. These data are also consistent with recent high-throughput *S. aureus* mutant experiments, which show that *P. aeruginosa* imparts significant stress on *S. aureus* in co-infected murine wounds (103).

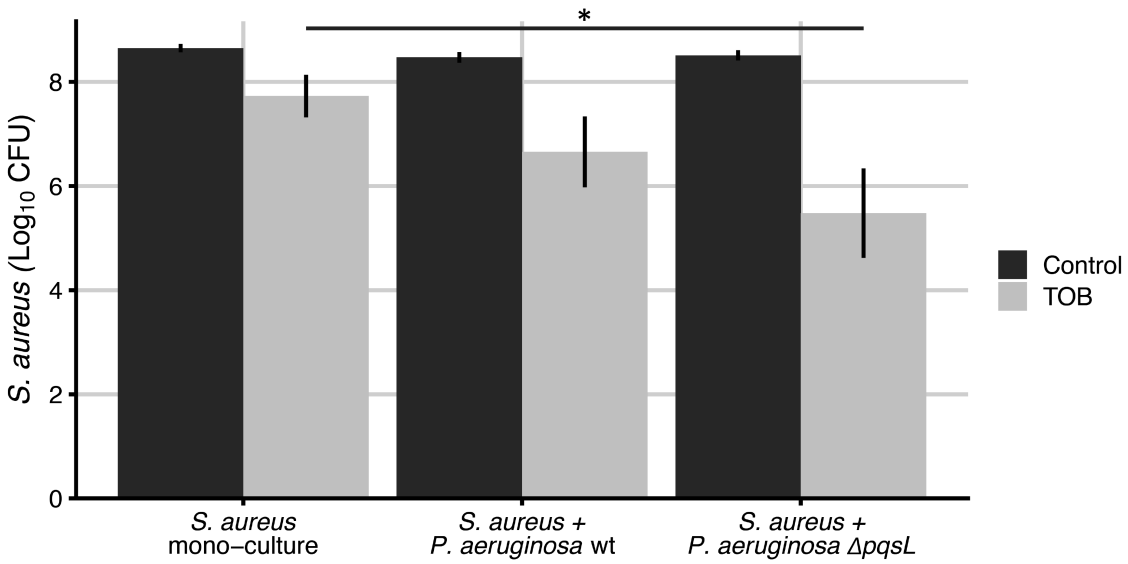

Figure 2-6 HQNO enhances S. aureus survival to tobramycin during coculture.

S. aureus was grown in SCFM2 under three conditions: monoculture, coculture with *P. aeruginosa*, and coculture with *P. aeruginosa ΔpqsL*. Cultures were then treated with tobramycin (256 μg/ml) or water (control), and the number of *S. aureus* CFU was determined. ($n = 12$; *, $P < 0.05$ by the Kruskal-Wallis test, followed by a *post hoc* paired Wilcoxon test). Error bars indicate standard deviations.

2.3 Conclusions

Our studies reveal that static growth in SCFM2 allows for long-term co-culture of *S. aureus* with a strain of *P. aeruginosa* that has high anti-staphylococcal activity under well-mixed conditions. Based on this study and our previous findings that SCFM2 is a biologically relevant model for studying CF lung infections (59, 61, 124-126), we propose that this co-culture model provides a means to study interactions between *S. aureus*, *P. aeruginosa*, and potentially other bacteria infecting the CF lung. Our results also reveal that elimination of HQNO has no effect on the fitness of *S. aureus* or *P. aeruginosa* during static co-culture relative to mono-culture but does impact spatial organization and susceptibility to tobramycin. These data may be particularly meaningful for co-culture studies including those in animals, as bacterial numbers (fitness) are often the primary data used to identify interactions and assess the relevance of specific pathways on bacterial interactions. We propose that assessing spatial organization of communities may be as informative as assessing fitness, and that the use of straightforward pipelines for quantifying spatial structure will be critical for understanding the functions of human-associated microbial communities.

While our study focused on laboratory strains of *P. aeruginosa* and *S. aureus*, it is clear that the genotype of the strains used can impact relative fitness during co-culture (108, 123, 137). Although we anticipate that relative fitness might be impacted by the use of other strains, as *P. aeruginosa* PA14 is highly lytic for *S. aureus* LAC under well-mixed conditions, their survival in static SCFM2 indicates that this model will likely promote co-existence for multiple genotypes, even those that are highly antagonistic. Finally, it was previously suggested that SCFM2 does not support robust co-existence of *P. aeruginosa*

and *S. aureus*, even under static growth conditions (90). However, in this previous study the static assay quantified bacteria that remained attached to the well of a 96-well plastic dish after vigorous washing, ultimately demonstrating that *P. aeruginosa* was ~100-fold more prevalent than *S. aureus* after 12 hours. The likely reason these results differ from ours is that most of the bacteria in SCFM2 grow as suspended aggregates and planktonic cells (59, 61), and we have not focused on the bacteria attached to surfaces as our goal is to model human infection. In addition, the fact that this previous study observed ~10^7 bacteria attached to the plastic surface at 12 hours (90) reveals that only about 1% of the total number of bacteria in the co-culture were growing attached to plastic as the carrying capacity of *P. aeruginosa* in SCFM2 is >10^9 CFU/mL (Fig. 2-1A&B). Ultimately, our results provide strong evidence that static growth in SCFM2 supports co-existence of *P. aeruginosa* and *S. aureus* and provides the opportunity to study interactions between these common co-inhabitants of human infections.

2.4 Methods

2.4.1 Strains, media and growth conditions

Prior to use, strains were streaked on tryptic soy agar plates (Sigma) then inoculated into tryptic soy broth and grown overnight at 37°C with shaking at 250 rpm. Wild-type *P. aeruginosa* strain PA14 and PA14 *ΔpqsL* were fluorescently labeled with the GFP-expressing plasmid pMRP9-1 (138) and maintained with 100 ug/ml of carbenicillin. *S. aureus* LAC was fluorescently labeled by moving pHC48 (139), containing dsRed under the control of the *sarA* promoter, from RN4220 by phage transduction. *S. aureus* carrying pHC48 was cultured with 10 ug/ml of chloramphenicol to maintain the plasmid.

2.4.2 Construction of the *P. aeruginosa* PA14 *pqsL* deletion mutant

A *pqsL* deletion mutant was constructed in PA14 by removing the gene *pqsL* by homologous recombination. The knockout construct was made by amplifying approximately 1 kb DNA fragments upstream and downstream of *pqsL* with overlapping sequences and ligating these fragments into pEXG2 (Promega) using Gibson assembly to form pEXG2pq. Primer sequences to PCR amplify the *pqsL* upstream region were tcggtacccggggatcctctggtgttcaacgtggtccc and aggaacgctcGCAGCCGTTGATCAGTAC and for amplification of the *pqsL* downstream region were caacggctgcgagcgttcctatcagccg and catgcctgcaggtcgactctGTGTTCCTCAATCTGCTGC (capital letters indicate bases that anneal to the *P. aeruginosa* target region and lowercase correspond to overhang sequences used for Gibson assembly). For linearizing pEXG2, we used the primers GCTTTACATTTATGCTTCC and ATGATCGTGCTCCTGTCG. The fragments were combined using Gibson assembly, and the resulting ~7 kb plasmid (pEXG2pq) was purified and transformed into *Escherichia coli* DH5α using the Transformation and Storage Solution (TSS) method (140) and selected on 15 µg/ml gentamicin. The plasmid was then purified and transformed into *E. coli* SM10 *λpir* using the TSS method (140) and selected on 15 µg/ml gentamicin. The knockout vector (pEXG2pq) was conjugated into *P. aeruginosa* as previously described (141). *E. coli* was counter-selected using *Pseudomonas* Isolation Agar plates (Sigma) and *P. aeruginosa* recombinants were selected with 60 µg/ml gentamicin. Forty-eight colonies were screened for sensitivity to sucrose. Allelic replacement was confirmed by PCR and phenotypically by identifying colonies that exhibit autolysis (142).

2.4.3 Complementation of P. aeruginosa PA14 *ΔpqsL*

pqsL was amplified with the Expand Long Template PCR system (Sigma) from *P. aeruginosa* PA14 chromosomal DNA using the forward primer 5'-GAATTCGGAACGACACGGAGACTCATCC-3' and reverse primer 5'-GAGCTCAGCCGCGCGGAGC-3'. The 1238 bp amplicon was ligated into the TOPO cloning vector using the TOPO TA cloning kit (ThermoFisher) to create pTOPO-pqsL. *pqsL* was then removed from pTOPO-pqsL by EcoR1 digestion and cloned into EcoR1-digested pBBR1MSC-5 (143). In the resulting plasmid (pBBR1-pqsL), *pqsL* is oriented such that it is transcribed from the *lac* promoter.

2.4.4 Growth in SCFM2

Overnight cultures of *P. aeruginosa* and *S. aureus* were sub-cultured in SCFM (109) until they reached exponential phase (OD_{600} of 0.3-0.6). Cultures were then washed and concentrated in pre-warmed SCFM without antibiotics to an OD_{600} of 1.0. These cultures were then used to inoculate each bacterium into SCFM2 at an OD_{600} of 0.05 in mono- or co-culture. 300 µl inoculated SCFM2 was then placed into wells of an 8-well optical chamber (Nunc™ Lab-Tek™ Chambered Coverglass) and incubated statically or well-mixed at 37°C. Well-mixed cultures included a magnetic stir bar (1.5 x 8 mm) in each of the wells rotating at 250 rpm. Growth was assessed at 4 hours intervals (4, 8, 12 and 16) using dilution plating with *P. aeruginosa*- and *S. aureus*-selective media, *Pseudomonas* Isolation agar and Baird-Parker Agar, respectively.

2.4.5 Disc diffusion assays

For the supernatant assays, *P. aeruginosa* cultures were grown as described above in SCFM2. After 16 hours, cultures were centrifuged at 5000 rpm for 10 min, and

supernatants were filtered through a 0.45 µm syringe filter and placed on ice. Overnight cultures of *S. aureus* were spread on BHI plates using sterile swabs, 6-mm filter paper discs were placed onto the agar, and 10 µl of either *P. aeruginosa* supernatant or SCFM2 (as a control) was added to each disc and allowed to dry at room temperature. The zone of inhibition was measured after 24 hours of incubation at 37°C. To assess lysis by *P. aeruginosa* cells, instead of supernatant being added to a disc, 5 µl of planktonic BHI-grown P. aeruginosa (OD600 = 0.5) was added.

2.4.6 Tobramycin susceptibility assay

S. aureus was inoculated as described above in SCFM2 in mono-or co-culture with *P. aeruginosa*, grown statically for three hours, then treated with 256 µg/ml tobramycin for two hours. Surviving bacteria were quantified by dilution plating with *P. aeruginosa*- and *S. aureus*-selective media, *Pseudomonas* Isolation agar and Baird-Parker Agar, respectively.

2.4.7 CLSM imaging

The same SCFM2 culture methodology described above was used for imaging. Three wells (*S. aureus* mono-culture, *P. aeruginosa* mono-culture, and co-culture) per optical chamber were used for each replicate imaging experiment. Each experiment imaged a single position in each well, once per hour. All images were acquired with a Zeiss LSM 880 CLSM utilizing Zen image-capture software. Detection of DsRed-expressing *S. aureus* cells was performed with an excitation wavelength centered at 587 nm and an emission wavelength centered at 610 nm. Detection of GFP-expressing cells was performed using an excitation wavelength centered at 488 nm and an emission wavelength centered at 509

nm. All images were acquired using a 63X oil-immersion objective. All data were stored as 1024- by 1024-pixel slices in stacks of 91 8-bit images. Each voxel is 0.264x0.264x0.44 μm^3.

2.4.8 Image Thresholding

Confocal images were exported as a tiff stack and thresholded using MATLAB (Simulink). A threshold was identified for each image stack using Otsu's method (144). For each channel, the final threshold for all images was identified by calculating a trend line over time across all calculated thresholds and using the value at the median time point.

2.4.9 Calculating aggregate size and histograms

Binarized image stacks were imported as a 3D matrix and segmented using the *bwconncomp* function (MATLAB R2019a, Simulink), finding connected voxels with 18-level connectivity (identifying voxels that touch at one of their faces or edges). The size of each object was mapped from voxels to μm^3, and a histogram with a 5 μm^3 bin size was created using a custom script in R (version 3.6.1

2.4.10 Determination of single vs. multi-species aggregates

To identify multi-species aggregates, co-cultured binarized image slices with *S. aureus* in the red channel and *P. aeruginosa* in the green channel were converted to grayscale images using im2bw function and segmented using the *labels* function to identify connected pixels in 2 dimensions of bacterial biomass, independent of species (MATLAB R2019a, Simulink). Those bacterial segments create a bacterial objects matrix. Two more matrices were created; one for *P. aeruginosa* (green channel) and another for *S. aureus*

(red channel). The bacterial matrix was then combined with either the green or red matrix from the same image to characterize the composition of bacterial segments in regard to species-specific segments. Bacterial aggregates composed of more than one channel were considered multi-species aggregates.

2.4.11 Calculating Proportional Occupancy and Enrichment Distance

To determine proportional occupancy, binarized image stacks were analyzed using a custom pipeline developed in R (publicly available at https://jupabago.github.io/PaSaProject/). Briefly, a focal voxel in the 3D image was picked at random and the voxels of a specific channel that were located within a spherical distance interval away (between radius 1 and radius 2) from the focal voxel were counted. Proportional occupancy was calculated by multiplying the number of voxels within a distance interval by the size of each voxel, divided by the total volume of the spherical shell bound by that distance interval:

$$Proportional\ Occupancy = \frac{number\ of\ voxels\ in\ distance\ interval\ \times\ voxel\ volume}{total\ volume\ of\ interval}$$

Proportional occupancy was obtained for 5,000 random focal voxels per image, starting from a distance of 1 μm away from each focal voxel and continuing for 30 μm using 1 μm distance intervals. When the focal voxel picked at random was located closer than 30 μm the edge of the image, the proportional occupancy was corrected by using the volume of shells from a capped sphere instead of spherical shells. Proportional occupancy was calculated using *S. aureus* as a focal point and using *S. aureus* (control) or *P.*

aeruginosa as surrounding cells. For the 5000 random focal voxels, a histogram of proportional occupancy values was produced at each distance. The proportional occupancy was calculated for each distance interval as the weighted median, and the distance interval with the highest weighted median is the enrichment distance.

CHAPTER 3. IMPACT OF HOSTILE INTERACTIONS WITHIN PATHOGENS DURING CHRONIC INFECTION

3.1 Introduction

Human infections caused by more than one microbial species pose a major burden on human health. They are typically more tolerant to antibiotics and have worse clinical outcomes compared to their single-microbe counterparts (65, 95). Properties specific to polymicrobial infections are often attributed to interactions occurring between microbes, and much work has been done to identify and mechanistically understand these interactions (80, 103-105, 145). *Pseudomonas aeruginosa* and *Staphylococcus aureus* have been used together as a model community to study these interactions because they cause polymicrobial infections in several sites, including chronic wounds and the lungs of people with cystic fibrosis. *P. aeruginosa* is a Gram-negative opportunistic pathogen that primarily causes infections in people with comorbidities like diabetes, immunodeficiencies or cystic fibrosis. (96, 97). *S. aureus* is a Gram-positive opportunistic pathogen with an increasing number of strains becoming antibiotic resistant. Infections with both these microbes display common signs of synergy, including increased antibiotic tolerance and heightened clinical outcomes (68, 80). Although they commonly coexist in multiple infection types, coexistence does not occur in most laboratory conditions, suggesting their interactions are fundamentally dictated by their environment. As a result, characterized interactions *in vitro* are limited and their relevance to infection environment are not well understood, and few studies have looked at interactions *in vivo*. Thus, it is still an open question what the nature and the magnitude of their interactions during infection is.

From an ecological standpoint, the first step towards understanding a community is to observe their members in their native environment and identify characteristics like the overall abundance of each species, the groups they form and their distribution in space. Communities in polymicrobial infections are an ideal system to be studied under this light. Unlike macro-scale communities, there is a clear community function that is quantifiable, the ability to cause disease; every individual in the community can be counted and community members can be genetically modified to obtain mechanistic insight for community dynamics. In these chapter I, describe work aimed towards understanding interactions of *P. aeruginosa* and *S. aureus* model community by characterizing their microbiogeography in a mouse chronic wound infection model. This model was chosen because it closely recapitulates the metabolism of *P. aeruginosa* in human infections (125). Previous observations broadly surveyed the spatial structure of mouse chronic wounds infected with *P. aeruginosa* and *S. aureus* and concluded these microbes segregated and were found in different locations within the wound (6). We hypothesize that these microbes are spatially organized in the wound, and they are interacting via specific molecules that modulate their spatial structure. To test this hypothesis, I captured images of wounds infected with of *P. aeruginosa* and *S. aureus* and analyzed them in a framework I developed. To gain mechanistic understanding of these interactions, I used strains of *P. aeruginosa* that cannot produce either HQNO or pyocyanin, metabolites produced by *P. aeruginosa* that have been shown in vitro to affect respiration of *S. aureus* and impact its metabolism and antibiotic susceptibility(68, 146).

3.2 Results

3.2.1 Early observations and study design

To study the interactions between *P. aeruginosa* and *S. aureus* and how they shape the spatial structure of an infection, I used confocal microscopy to image mono and co-culture mouse chronic wounds infections of fluorescently labeled strains. The chronic wound model consists of a 2-cm radius circular surgical incision in the back of a mouse (6). For these experiment, half of the wound was used for either CFUs or RNA-seq analysis performed by another lab member, and I used the other half for imaging. Additionally, early observations of wounds under the microscope revealed a high heterogeneity in bacterial density across the wound and qualitative differences among different regions the wound. Thus, I decided to photograph the objective over the wound each time a confocal image was taken. This resulted in matched confocal images with wound region photographs. I then used the photograph to classified image as core or edge, depending on the region of the wound being imaged because those classifications were simple and yet captured the observed heterogeneity. This allows for exploration of spatial structure at both the micron scale and the "milli-scale." The local heterogeneity involved vast areas without any visible bacteria cells contrasted with highly dense areas. To capture this heterogeneity, the size of the confocal images varied depending on the area sampled and ranged from squares 250 μm by 250 μm (.0625 cm), to larger rectangles of up to 800 μm by 200 μm (.16 cm2), which accounts for 1 to 3% of the total area of the wound. Each wound was imaged in three or more different locations and at least three wounds were imaged per condition, resulting in a total of 110 images. The imaging protocols were optimized to capture inter-sample variability. The sample treatment was minimal to preserve the spatial

patterns in the wound and minimize the disturbances to the local and global wound environment.

3.2.2 *P. aeruginosa* impacts the aggregation of *S. aureus* in chronic wounds.

The first question to answer was, how well the images recapitulate data from CFU counts? Those measurements were collected by Carolyn Ibberson (Appendix Fig S-2), a fellow lab member indicated that *P. aeruginosa* was more fit in mono-culture compared to co-culture, while *S. aureus* showed no difference between conditions. Figure 3-1A shows the total biomass obtained from image analysis. I found no significant difference in the total biomass between mono and co-culture of either *P. aeruginosa* or *S. aureus,* but images of *P. aeruginosa* in mono-culture showed the highest biomass, while co-culture samples showed the lowest. I also compared biomass from samples at different regions, edge vs core. No significant difference was found within co-culture samples, and *S. aureus* mono-culture only had only two samples at the edge, which is not enough for statistical significance, but the lowest biomass for *S. aureus* was observed in images from edge of the wound. These results indicated the samples partially captured the global patterns of abundance in viable cells observed in CFU counts, but the local environment within each wound may provide a better understanding of interaction dynamics between *P. aeruginosa* and *S. aureus* in the chronic mouse wound.

Thus, I moved forward with the characterization of metrics related to spatial structure and the first question was how is the biomass distributed in the wound? To answer this question, I first counted the groups of bacteria found in the infections. Figure 3-1B shows the total number of groups of bacteria for *P. aeruginosa* and *S. aureus*. A group of bacteria

is composed of neighboring voxels that belong to the same species. I found no difference in total groups of bacteria independent of region between mono and co-culture in either *P. aeruginosa* or *S. aureus*. However, region classification showed *S. aureus* at the edge have more groups, 7206 on average, than the core, 1970, in co-culture with *P. aeruginosa* (*p*-value = 0.06). The same was true for *P. aeruginosa* in co-culture with *S. aureus*, with mean values of 1788 and 6930 for core and edge respectively (p-value = 0.02). These results suggest that while there is no observable difference in total biomass between regions, its distribution is different. Closer observations showed the size of these groups spanned a large range of values and these difference in sizes and overall frequency may impact the dynamics of the interactions between these species.

Bacteria in different group sizes are classified primarily as either planktonic cells or aggregates in the context of infectious diseases. This classification has been associated with several metrics, including dispersal, antibiotic susceptibility, and overall fitness(59, 147, 148). The next question was, are these microbes growing as planktonic cells or aggregates, and how large are those aggregates? To answer this question, I classified the groups of bacteria according to their size and calculated the relative frequency of each size range. I used five different bins, corresponding to volume ranges, to capture the wide spectrum of observed group sizes. The bin for smallest size was from 0.5 to 5 μm^3 and corresponds to planktonic cells (59). The other bins were 5 to 10 μm^3, 10 to 100 μm^3, 100 to 1000 μm^3 and larger than 1000 μm^3, which are collectively known as aggregates. Figure 3-1C shows that on average 91% of *S. aureus* groups observed in co-culture are planktonic cells, compared to 46% in mono-culture (*p*-value <0.01). This increase in relative frequency of planktonic cells in co-culture was compensated by decrease in aggregates of the first two

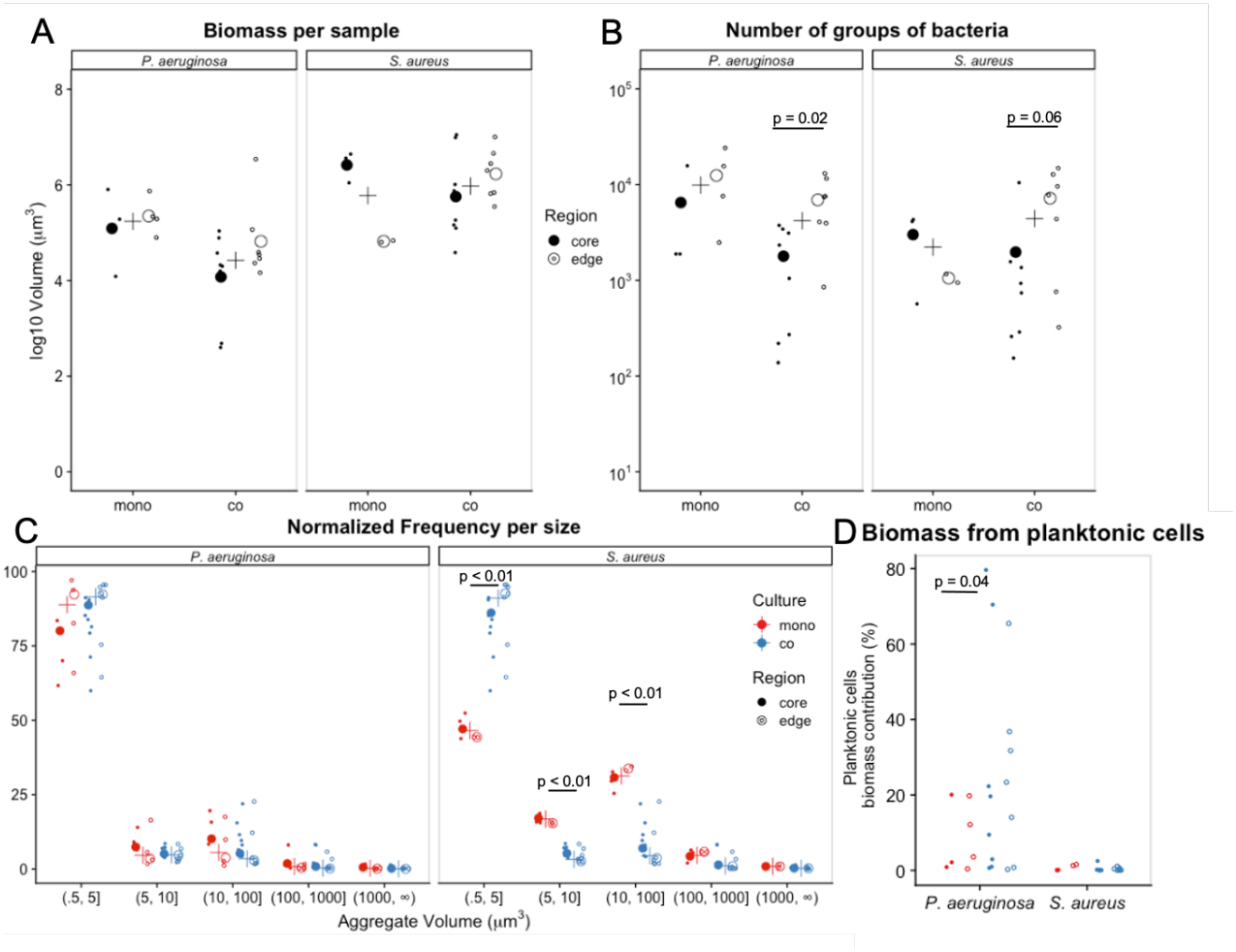

Figure 3-1 Spatial structure of *P. aeruginosa* and *S. aureus* in a mouse chronic wound.

(A)Total biomass from confocal images analysis of *P. aeruginosa* and *S. aureus* in mono and co-culture. (B) Number of bacterial groups identified from confocal images of *P. aeruginosa* and *S. aureus* in mono and co-culture. (C) Binned histogram of relative abundance of each group size of *P. aeruginosa* and *S. aureus* in mono and co-culture.(D) Biomass contribution from planktonic cells of *P. aeruginosa* and *S. aureus* in mono and co-culture. The crosses indicate the mean across all samples, filled circles indicate samples from core region and empty circles from edge region. Large circles represent the mean for the samples of the region they represent. P-values calculated using unpaired Student's t-Test

size ranges. Consequently, the relative frequency of aggregates in the 5 to 10 μm^3 and 10 to 100 μm^3 size ranges was higher, 16% and 31%, for *S. aureus* in mono-culture compared to co-culture with *P. aeruginosa*, 3% and 4% respectively. (p-value < 0.01). The data also shows *S. aureus* aggregates at the 10 to 100 μm^3 bin are over-represented compared to the other sizes, and to the same bin in *P. aeruginosa*; this size has been hypothesized to be more fit against uptake by phagocytes (149). *P. aeruginosa* was found to be largely planktonic cells and unaffected by co-culture with *S. aureus*. The data suggest that *P. aeruginosa* may be influencing *S. aureus* either directly or indirectly towards a planktonic lifestyle, a phenotype that has been shown to happen *in vitro* at a the colony scale (118). However, the large range in size of bacterial groups prevents from drawing a conclusion about the overall impact of the shift towards planktonic life. Additionally, data from Chapter 2 indicated that *S. aureus* exists largely as aggregates. So next, I looked at how much of the total biomass is found as planktonic cells in mouse chronic wounds. Figure 3-1D shows *S. aureus* primarily exists as aggregates and planktonic cells contribute to 1% or less of the total biomass. Additionally, it shows that planktonic cells can contribute to up to 80% of total biomass of *P. aeruginosa* and that this effect is more pronounced in co-culture with *S. aureus* as the mean contribution in mono-culture is 8% compared to 25% in co-culture (p-value = 0.04). The impact of both microbes on the aggregation and, consequently, on their life history during infection provides evidence these microbes are interacting in this environment either through direct or indirect mechanisms. Previous studies have identified effectors *P. aeruginosa* releases that influence this phenotype *in vitro* (68). Next, I tested whether the same mechanisms influence *S. aureus* in an infection environment.

3.2.3 Impact of HQNO and pyocyanin on interactions between *P. aeruginosa* and *S. aureus* in mouse chronic wounds

Most interactions between *P. aeruginosa* and *S. aureus* are thought to be hostile, so we hypothesized that *P. aeruginosa*-secreted HQNO and pyocyanin can mediate this interaction. Both molecules have been found to impact physiology and fitness of *S. aureus* (68, 146). To test if the release of these molecules drives interactions found in wounds, two more fluorescently labeled strains of *P. aeruginosa* were used to infect mice: a strain with deletion of *pqsL* gene and unable to produce HQNO, and a strain with *phz1/2* deletions and unable to produce pyocyanin. I applied the same imaging protocol and analysis framework as before to infections with *P. aeruginosa* Δ*pqsL* and *P. aeruginosa* Δ*phz1/2* in mono and co-culture with *S. aureus*. Figure 3-2A shows the total biomass of *S. aureus* in co-culture with wild type *P. aeruginosa,* Δ*pqsL* and Δ*phz1/2*. No change in biomass was found for *S. aureus* in co-culture with either mutant compared to wild-type and *S. aureus* was also found in the edge and the core of the wounds at equivalent magnitudes in co-culture with both mutant strains. Additionally, there was no observed difference in fitness for either *P. aeruginosa* Δ*pqsL* or *P. aeruginosa* Δ*phz1/2* compared to the wild-type, suggesting these mechanisms do not influence the overall fitness of *P. aeruginosa* in co-culture with *S. aureus* in the chronic wound environment.

Next, I counted the total groups of bacteria in each condition. Figure 3-2B shows the number of groups increased for *S. aureus* in co-culture with wild type, 4,413 compared to the Δ*pqsL* strain 11,122 (p-value = 0.03). For *P. aeruginosa* strains in co-culture with *S. aureus,* both mutant strains Δ*pqsL* and Δ*phz1/2* had higher mean number of cell groups 11,784 and 16,255, compared to the wild type 4,188 (p-value = 0.06 and < 0.01,

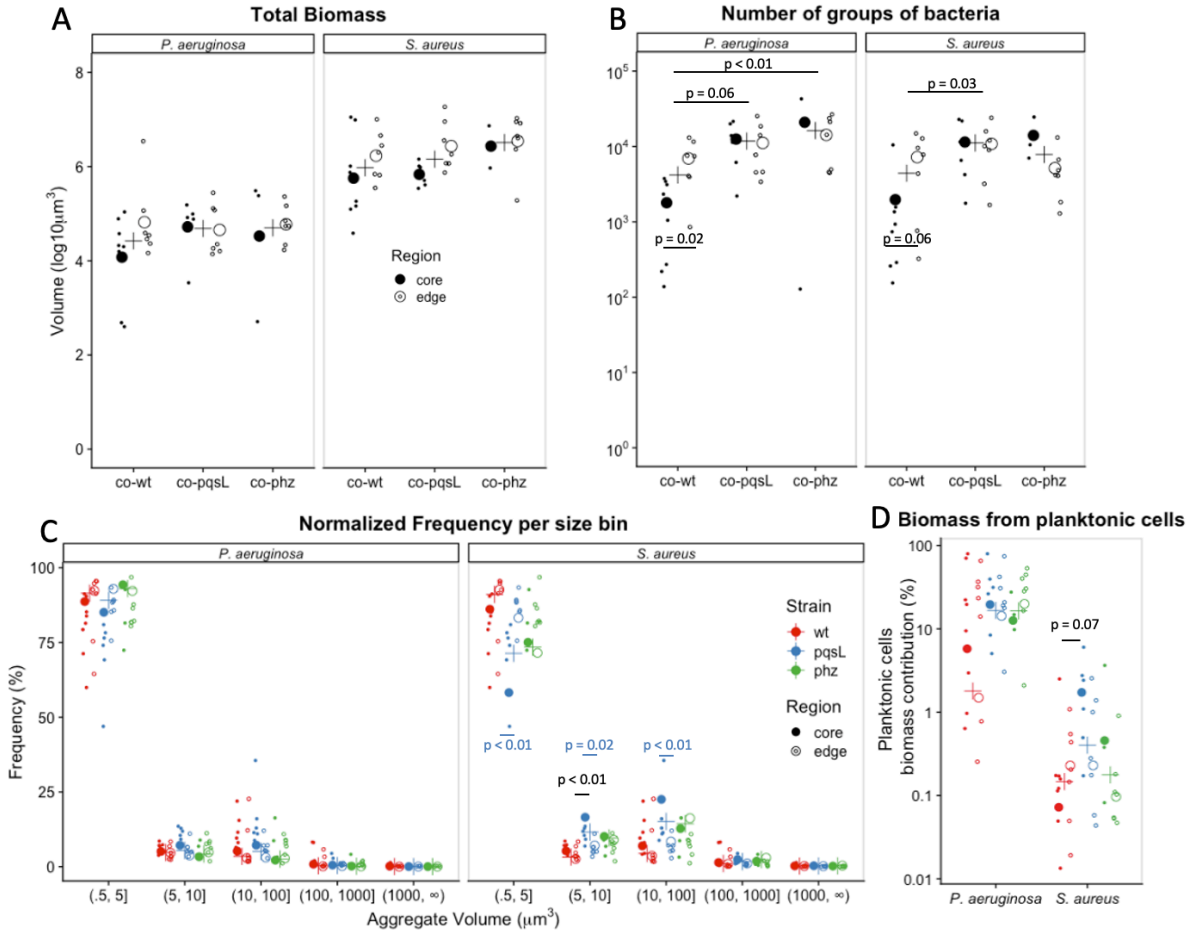

Figure 3-2 Spatial structure of *S. aureus* in co-culture with *P. aeruginosa* wild type, Δ*pqsL* and Δ*phz1/2* in mouse chronic wound

(A) Total biomass from confocal images analysis of *S. aureus* in co-culture with *P. aeruginosa* wild type, Δ*pqsL* and Δ*phz1/2*. (B) Number of bacterial groups identified from confocal images of *S. aureus* in co-culture with *P. aeruginosa* wild type, Δ*pqsL* and Δ*phz1/2*. (C) Binned histogram of relative abundance of each group size of *S. aureus* in co-culture with *P. aeruginosa* wild type, Δ*pqsL* and Δ*phz1/2* (D) Biomass contribution from planktonic cells of *S. aureus* in co-culture with *P. aeruginosa* wild type, Δ*pqsL* and Δ*phz1/2*. The crosses indicate the mean across all samples, filled circles indicate samples from core region and empty circles from edge region. Large circles represent the mean for the samples of the region they represent. P-values calculated using unpaired Student's t-Test or ANOVA one way for multiple comparison tests followed by Tukey HSD.

respectively). There was no observed difference in number of groups for either species related to region of the wound. The difference in groups of bacteria found in both Δ*pqsL* and Δ*phz1/2 P. aeruginosa* shows these mechanisms can modulate aggregation in *P. aeruginosa* and its overall physiology in the presence of *S. aureus*.

Next, I looked at the relative frequency of groups of different sizes using the ranges established in the previous section. Figure 3-2C shows the frequency of *S. aureus* planktonic cells did not significantly changed in co-culture with wild-type *P. aeruginosa* compared to either Δ*pqsL* or Δ*phz1/2* strains, even though the average values where lower for both mutants. However, there was an observed increase in frequency in the 5 to 10 μm^3 bin for *S. aureus* in co-culture with *P. aeruginosa* Δ*pqsL* compared to the wild type. Additionally, differences between regions were observed for *S. aureus* in co-culture with *P. aeruginosa* Δ*pqsL* across different size bins. Planktonic cells of *S. aureus* were more frequently found in the edge vs core, while aggregates in both 5 to 10 μm^3 and 10 to 100 μm^3 were more frequent at the core than the edge (p-value <0.02 in all cases). Moreover, comparing each region and strain independently, I found frequency of *S. aureus* aggregates of size 10 to 100 μm^3 was higher than those in both core and edge of *P. aeruginosa* wild-type and the edge of *P. aeruginosa* Δ*phz1/2* (p-value<0.03, ANOVA one-way followed by Tukey HSD). This suggests that HQNO has an overall impact on aggregate size of *S. aureus* and this phenotype is variable across regions of the wound.

Lastly, I looked at the impact of HQNO and pyocyanin on contribution of planktonic cells to total biomass (Figure 3-2D). The highest contribution to planktonic cells of *S. aureus* across all co-culture conditions was found in with *P. aeruginosa* Δ*pqsL* and was significantly higher than *P. aeruginosa* wildtype (p-*value* = 0.07). This suggests that the

overall impact of *P. aeruginosa* to aggregation *S. aureus* in the wound environment is not limited to HQNO or pyocyanin.

3.2.4 Distribution of biomass across depths of chronic wounds

Mouse chronic wounds are shaped like discs; depth is vastly shorter than radius. While the z-dimension is significantly shorter than x and y, its impact may be disproportional to its size. Depth in wounds is related to exposure to the environment and may contribute to chemical gradients. To identify the role of depth on fitness of the community, I calculated the relative biomass at each slice of the confocal image.

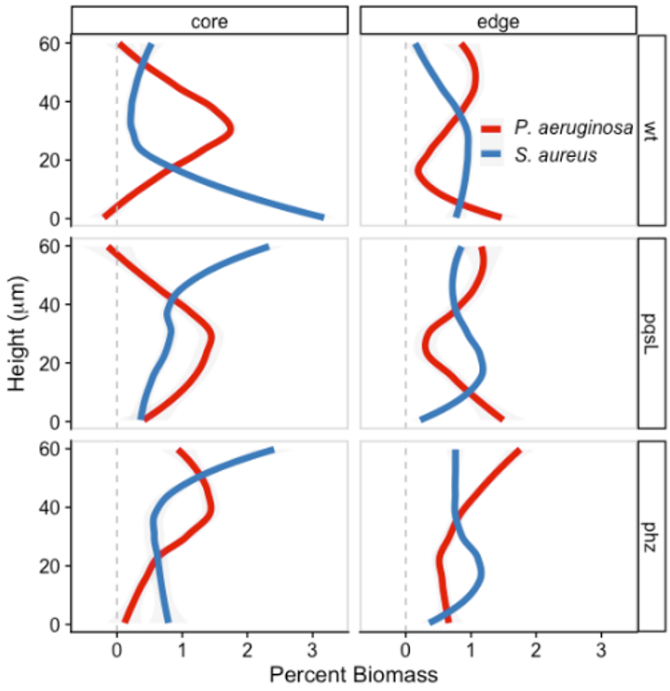

Figure 3-3 Biomass of *P. aeruginosa* and *S. aureus* in co-culture as a function of tissue depth.

The height at zero is the surface of the wound and increasing numbers denote tissue depth. *P. aeruginosa* is shown in red and *S. aureus* is shown in blue. Each block represents a different region-strain combination.

Figure 3-3 shows the normalized biomass found at different depths of the wound, from the surface, at zero height, up to 60 μm into the tissue. For *S. aureus*, co-culture with wild type or mutant does not change the biomass distribution at the edges, but at the core, *S. aureus* in co-culture with wild type most biomass is found 30 μm within the surface, while for the mutants it is deeper in the tissue. For *P. aeruginosa*, we found that core and edge samples have the reverse trend, where most of the biomass in the core samples is found around 30 μm into the tissue, while at the edge the biomass is found either deeper into the tissues or at the surface. While these result show that there is an interaction between *P. aeruginosa* and *S. aureus* mediated in part by HQNO and pyocyanin, the micron scale spatial structure may provide more data to characterize the impact of these metabolites on these interactions.

3.2.5 Micron-scale spatial structure

An additional goal of this work was to observe the micron-scale spatial organization of the *P. aeruginosa*-*S. aureus* model microbial community in a minimally disturbed chronic infection environment. To do this, I calculated the proportional occupancy (PO), which was also described in Chapter 2. In brief, it aims to characterize bacterial density in the immediate surrounding of a randomly chosen unit of bacterial biomass at discrete distance intervals. Figure 3-4A shows the calculated PO of *S. aureus* around randomly sampled voxels with *P. aeruginosa*. I focused on analysis centered at *P. aeruginosa* because we observed more *S. aureus* than *P. aeruginosa* in the chronic wounds; selecting the scarce species and counting the more abundant species provides a more representative assessment of the environment. The curve for *S. aureus* around *P. aeruginosa* wild type shows a positive correlation of distance with PO, suggesting an active segregation

mechanism, as shown in a previous study I was involved (55). In contrast, the curves for both Δ*pqsL* and Δ*phz1/2* mutants show a different shape with the positive correlation of PO is followed by stabilization at a constant PO value, indicating an enrichment at specific distances. These data indicate that the spatial structure of the *P. aeruginosa*-*S. aureus* microbial community in a mouse chronic wound can be modulated by small molecules released by community members.

To further describe the differences of spatial structure between communities with different strains of *P. aeruginosa*, I calculated the enrichment distance; the distance at which the proportional occupancy is the highest. Figure 3-4B shows the enrichment distance of *S. aureus* around different strains of *P. aeruginosa*. The shortest enrichment distance was with *P. aeruginosa* Δ*pqsL* at 12 +/- 3 μm and was significantly different from that of *P. aeruginosa* wild type at 22 μm (*p*-value 0.03, unpaired Student's t-test). No difference was found for *P. aeruginosa* Δ*phz1/*2. This shows that *P. aeruginosa*-released HQNO increases the distance between *S. aureus* and *P. aeruginosa* in a mouse chronic wound infection model.

In addition to using PO to calculate enrichment distance between species, I also calculated the empty space around each species by adding PO values centered at one species and subtracting them from 1, the maximum value for PO. Figure 3-4C shows the empty space around all strains of *P. aeruginosa* increases with distance at short distances, but after 5 μm it stays constant. This suggests this value may have an overall significance in the spatial structure of the community. The figure also shows more empty space around both Δ*pqsL* and Δ*phz1/2 P. aeruginosa* mutant strains than the wild-type. These results indicate that even though the absence of HQNO and phenazine produce different

enrichment distances, the overall saturation of the environment around both mutants is constant.

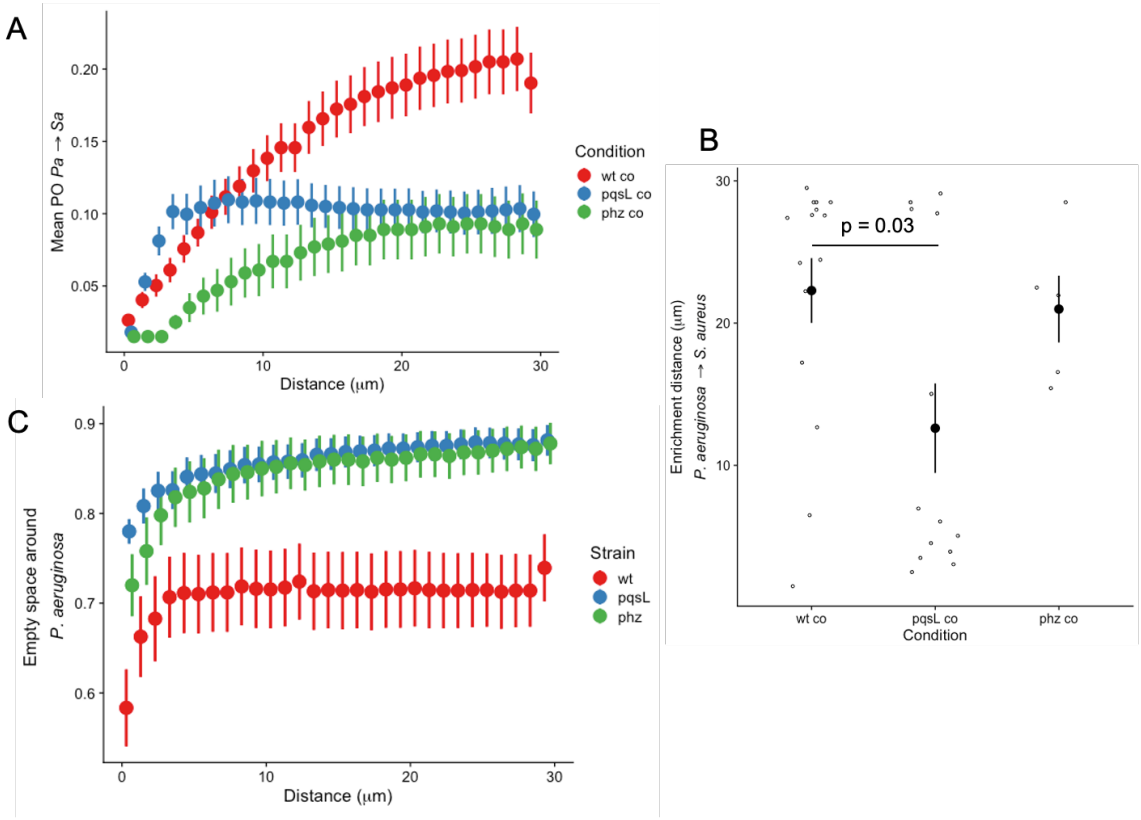

Figure 3-4 Micron-scale spatial organization of *S. aureus* in co-culture with *P. aeruginosa* wild type, Δ*pqsL* and Δ*phz1/2* in mouse chronic wound

(A) Proportional occupancy of *S. aureus* surrounding different strains of *P. aeruginosa.* The curve for *S. aureus* around *P. aeruginosa* wild type shows a positive correlation of distance with PO, while the curves for both Δ*pqsL* and Δ*phz1/2* show a different shape with the positive correlation of PO is followed by stabilization at a constant PO value (B) Enrichment distance of *S. aureus* from different strains of *P. aeruginosa.* The shortest enrichment distance was with *P. aeruginosa* Δ*pqsL* at 12 +/- 3 μm and was significantly different from that of *P. aeruginosa* wild type at 22 μm(*p*-value 0.03, unpaired Student's t-test). No difference was found for *P. aeruginosa* Δ*phz1/2*. (C) Empty space around all strains of *P. aeruginosa* increases with distance at short distances, but after 5 μm it stays constant. Red represents *P. aeruginosa* wild type, blue represents *P. aeruginosa* Δ*pqsL* and green represents *P. aeruginosa* Δ*phz1/2.* Error bars represent standard error of the mean.

3.3 Discussion and conclusions

Polymicrobial infections are a fundamental issue in human health and subject to extensive research, primarily on understanding how co-infecting species respond to each other. While exploring the spectrum of possible interaction mechanisms between pathogens is important, little is known about whether those interactions take place at the infection site. Basic understanding about organisms can be drawn from observing patterns of abundance in their native environment, and yet only one other study has quantified spatial structure pathogens in an infection (83). The results shown here suggest that two co-infecting microbes that don't coexist under most laboratory conditions, *P. aeruginosa* and *S. aureus*, can be found within microns of each other in an infection. Moreover, the presence of *S. aureus* impacts fitness of *P. aeruginosa*, which can in turn influence aggregation and region where *S. aureus* is found. This effect and their micron scale spatial organization are at least partially modulated by *P. aeruginosa*-secreted molecules.

The increase in groups of both *S. aureus* and *P. aeruginosa* in co-culture found at the edge compared to the core was unexpected (Figure 3-1B). Although, planktonic cells only marginally contribute to total biomass of *S. aureus*, the increase biomass at the edge may be linked to increased number of planktonic cells in co-culture with *P. aeruginosa*. *P. aeruginosa* might trigger dispersal of *S. aureus* and enable it to reach higher densities at the edge of the wound, which has a larger surface area. Since both pyocyanin and HQNO target respiration in *S. aureus*, this effect might be a dispersal of *P. aeruginosa* triggered by increased competition for oxygen to maximize surface area to volume. Data about the differences of core and edge region of the wound on the host side may help characterize this phenomenon.

Another topic worth expanding upon is the shape of the proportional occupancy curve(Figure 3-4A), which portrays the tendency of bacteria to be found at specific distances. The trends between wild-type and Δ*pqsL P. aeruginosa* show different dynamics of spatial organization, the enrichment distance for Δ*pqsL P. aeruginosa* is shorter, but the magnitude of PO at distances larger than 15 μm is higher for the wild type strain. While the expectation would be for the area under all curves to be equivalent due to their equivalent biomass, this is not the case. Local spatial structure doesn't necessarily match global spatial structure, and *S. aureus* cells farther than 30 μm from *P. aeruginosa* are not included in this PO calculation. The 30-micron distance was chosen because most the depth of most images is no higher than 60 microns, so PO at higher distances would not be representative. Furthermore, the value reported per condition for PO at each distance is the mean of each sample's median value from the sampling population of 1000 voxels. Thus, the significance of the magnitude of PO is in context of the sampled population. In this case, the strengths of characterizing micron-scale spatial structure using PO limits its interpretation on global metrics. However, other effects influencing the magnitude of PO can be inferred with further analysis, as is the case for *P. aeruginosa* in empty space and the biomass contribution of planktonic cells, explained below

Differences in amount of empty space around *P. aeruginosa* wild-type compared to mutants might be associated with the increase in number of planktonic cells of *P. aeruginosa* in mutants. The overall number of groups of cells is higher and the biomass contributed by these entities is up to 10 times higher in the *P. aeruginosa* mutants compared to the wild type. Thus, the increased empty space around mutants may be linked to differential aggregation patterns of *P. aeruginosa*. This could also support the hypothesis

of pyocyanin and HQNO influencing competition for oxygen leading *S. aureus* to maximize surface area to volume upon *P. aeruginosa* challenge.

There were series of observations that I was not able to portray clearly in the text involving some samples showing a 20 to 30 μm gap across the depth of the wounds were bacteria of either species were not present. Efforts to depict that gap are shown in the section characterizing biomass across the depth(Figure 3-3), and in the specific case of samples from the edge of *P. aeruginosa* Δ*pqsL* this effect can be seen. More thought on how to effectively portray these effects must occur before publication.

Overall, these results indicate that *P. aeruginosa* and *S. aureus* interact via HQNO and pyocyanin in a mouse infection model that closely recapitulates metabolism of these pathogens in human infection. Work with other lab members have shown that *P. aeruginosa* increases *S. aureus* tolerance to tobramycin in intact wounds, but homogenization of wounds negates this effect. Those results further show the impact of spatial structure in community fitness and in overall infection treatment.

3.4 Methods

3.4.1 CLSM imaging

Wounds were obtained 4 days post infection, cut in half and one half was used for imaging. Wound was placed in an CoverWell™ Imaging Chamber Gasket and two drops of ProLong Glass Antifade Mountant with NucBlue was added to prevent it from fading and minimize drift during imaging. Wounds were incubated for 30 minutes at 4°C. Samples were then placed in the microscope with the surface of the wound facing the objective. All

images were acquired using a Zeiss LSM 880 CLSM utilizing Zen image-capture software with 3 different detectors. Detection of DsRed-expressing *S. aureus* cells was performed with an excitation wavelength centered at 587 nm and an emission wavelength centered at 610 nm. Detection of GFP-expressing cells was performed using an excitation wavelength centered at 488 nm and an emission wavelength centered at 509 nm. Detection of DAPI was performed exciting at 405 nm and detecting emission from 420 nm to 470 nm. All images were acquired using a 63X oil-immersion objective. The wound was scanned for fluorescence signal and imaging began after centering in a region of interest. Images captured using tiles had 10% overlap and were later stitched using ZEN blue software.

3.4.2 Image Thresholding

Confocal images were exported as a tiff stack and each channel was binarized using MATLAB (Simulink). Image analysis started using a histogram stretching routine to span the entire range of intensity values. These images were then passed through the Wiener filter routine, which identifies high contrast in a kernel and maintains it, while averaging low contrast areas. A threshold was then identified for the each channel whole stack using Otsu's method (144). Final images were generated by subtracting the the red channel, corresponding to DrRed from the green channel, corresponding to GFP.

3.4.3 Calculating aggregate size and histograms.

This analysis was performed using the same routines as those used in Chapter 2.

3.4.4 Proportional occupancy

Proportional occupancy was calculated as described in Chapter 2. The value from each image at each distance was calculated by binning the proportional occupancy values, which range from 0 to 1, in intervals of 0.01 units and calculating the value for 50% of the population of 1000 random samplings for PO. The mean value from each image per condition was reported as the final value.

3.4.5 Enrichment distance

The highest value for PO from each sample across all distances was collected. In cases where more than one distance had the highest value, the weighted mean was calculated for the distance, using the population density of each distance as the weight. The reported enrichment distance was the mean per condition.

3.4.6 Calculating bacterial biomass at different depths

Binarized images were imported in R (version 3.7) as matrices. Since different samples were imaged up to different depths, I restricted analysis to samples with at least 60 μm in depth. Image slices representing the first 60 μm were extracted from those samples and the total biomass corresponding to that section was calculated. Then, the biomass of each slice within a sample was divided by the total biomass of that sample and that resulted in normalized biomass per height.

CHAPTER 4. IMPACT OF NUTRIENT EXCHANGE IN SPATIAL ORGANIZATION OF AMICROBIAL COMMUNITY DURING INFECTION

4.1 Introduction

Microbes can modulate their metabolism to fit their environment (71, 80, 103, 150). This environment is influenced by abiotic factors like temperature and pH, and by co-existing organisms. During polymicrobial infections, the response of microbes to other microbes can result in nutrient exchange, leading to increased microbial fitness and aggravating clinical outcomes(65, 70). Many methods exist to characterize the extent of these responses. However, limited tools exist to characterize these responses in the native environment, particularly those resulting in nutrient exchange. In this chapter, we ask the question: can we identify nutrient exchange by analyzing images of the community in their native environment? To test this idea, I used a model system previously described in the Whiteley lab, composed of *Aggregatibacter actinomycetemcomitans* (*Aa*) and *Streptococcus gordonii* (*Sg*) in a mouse abscess model(70, 83). *Aa* is a Gram-negative opportunistic pathogen associated with aggressive periodontitis, a potent inflammation of the gums that can result in sudden tooth loss. While *Aa* is almost exclusively found in the pocket between the tooth and the gum, it is also been found in abscesses inside and outside the mouth(151). *Sg* is a Gram-positive early colonizer oral commensal that is typically harmless but can cause infections like endocarditis when it gains systemic access. We chose these microbes because they co-exist in the oral cavity and in infections outside the mouth, their interactions, including nutrient exchange, have been well-characterized under

laboratory conditions and they are maintained during infection using the mouse abscess model (70).

Sg releases lactate as by-product of its metabolism, which is preferentially consumed by *Aa* instead of other more energy rich metabolites like glucose and fructose(71). This is important as *Aa* grows significantly slower than *Sg* and other *Streptococci* in the oral cavity, so the cross-feeding allows *Aa* to survive in a highly competitive environment (70). *Sg* also secretes the antimicrobial H_2O_2 upon exposure to oxygen (152), which *Aa* can then decompose into oxygen and water. The released oxygen can be used by *Aa* for respiration, a mode of energy production that requires oxygen. Respiration results in higher energy yields than fermentation, which is the only energy production mode available for *Sg,* but it does not require oxygen. This relationship is referred to as cross-respiration(72). The outcome of these exchange results in a commensal facilitating an opportunistic pathogen, questioning the role of resident microbiota. While these microbial interactions are motivated by nutrient limitation in the environment, they also occur in limited space. This chapter explores the changes in spatial structure that arise from nutrient exchange in the model *Aa/Sg* community during abscess infection. The overall hypothesis is that nutrient limitation and competition is associated with a signature space modulation. In contrast to previous chapters, this is still an ongoing project, hence data collection and curation have not been finalized.

4.2 Results

4.2.1 *Sg* promotes growth of *Aa* in a mouse abscess model

Sg can facilitate growth of *Aa* during infection in a mouse abscess model via release of lactate that *Aa* uses to grow(70). In turn, *Aa* converts H_2O_2 into oxygen that can be used for respiration(72). To examine the role of nutrient exchange during infection, I performed a series of mouse abscess infections using *Sg* and strains of *Aa* with mutations in genes key for interactions, each in mono and co-culture. This model is biologically relevant because both *Aa* and *Sg* have been co-isolated from abscesses in the mouth and other tissues. To assess the impact of lactate exchange during infection, I used an *Aa* mutant that is unable to grow on lactate, *AaΔlctD*. To assess the impact of *Aa*-produced oxygen, I used a catalase mutant, *AaΔkatA,* which cannot convert H_2O_2 into O_2. Assessing the fitness of these two mutants in mono and co-infection may indicate the requirements for *Sg*-promoted facilitation of *Aa* during infection.

The abscesses were collected 3 days post infection and growth of *Aa* and *Sg* was first quantified by plating in selective media. I first compared growth of *Sg* in mono and co-culture with *Aa*, and both *AaΔlctD* and *AaΔkatA*. The results showed *Sg* fitness did not increase in co-culture with *Aa* and *AaΔlctD* compared to mono-culture, but growth with *AaΔkatA* was modestly increased compared to mono-culture (Figure 4-1A p-value = 0.04, unpaired t-test). To better understand the impact of different *Aa* mutants on *Sg*, I compared growth in co-culture across all *Aa* strains. In this case, *AaΔkatA* had a significant growth advantage over *AaΔlctD* (p-value = 0.03, ANOVA followed by Tukey HSD). These

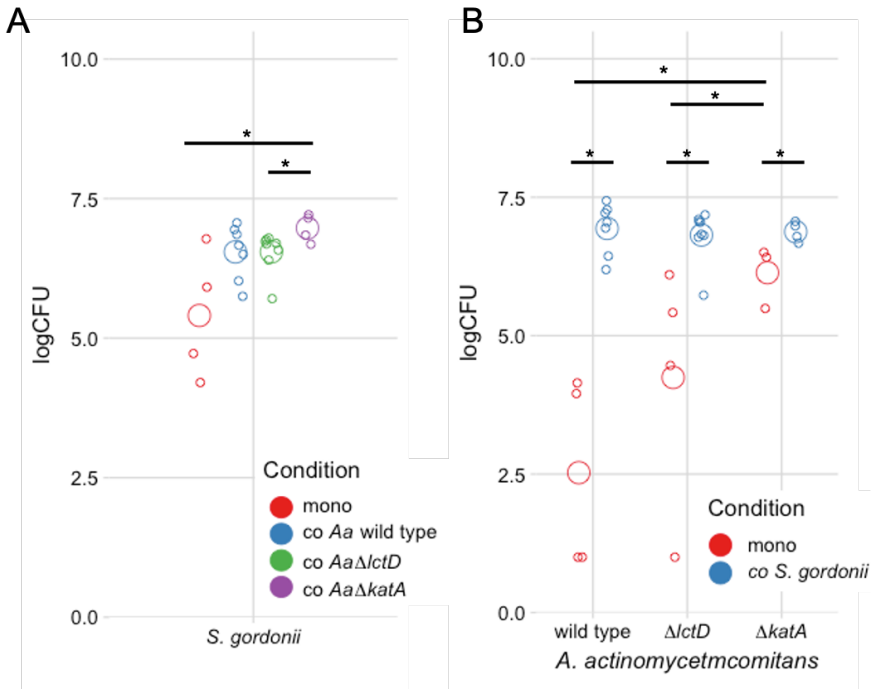

Figure 4-1Fitness of Sg and Aa wild type, *AaΔlctD* and *AaΔkatA* in mono and coculture using CFUs.

(A) Calculated growth from CFUs of *S. gordonii* in mono and co-culture with *Aa* wild type, *AaΔlctD* and *AaΔkatA*. Fitness of *Sg* did not increase in co-culture with *Aa* and *AaΔlctD* compared to mono-culture, but growth with *AaΔkatA* was modestly increased compared to mono-culture (p-value = 0.04, unpaired t-test). Additionally, *Sg* in co-culture with *AaΔkatA* had a significant growth advantage over *AaΔlctD* (p-value = 0.03, ANOVA followed by Tukey HSD). (B) All *Aa* strains incurred a fitness benefit from co-culture with *Sg* compared to mono-culture (pairwise comparisons, unpaired Student's t-test, $p<0.05$). Comparing *Aa* strains in mono-culture, *AaΔkatA* grew significantly higher than both *Aa* and *AaΔlctD* (* denotes p-value < 0.05, ANOVA one-way).

findings suggest that presence of *Aa alone* does not benefit *Sg*, but its ability to decompose H_2O_2 can dictate the fitness outcome of interaction for *Sg*.

I then looked at growth of *Aa* and its mutant strains in mono and co-culture with *Sg*. In mono-culture, *AaΔkatA* grew significantly higher than *Aa* (Figure 4-1B, p-value < 0.05, ANOVA one-way). Additionally, all strains of *Aa* incurred a fitness benefit from co-culture with *Sg* and ultimately reached equivalent levels. *Aa* increased 5 logs (Figure 4-1B, p-value 0.01), *AaΔlctD* increased 100-fold (*p*-value>0.01) and *AaΔkatA* had a small but significant increase from $10^{6.1}$ to $10^{6.8}$ CFU (*p*-value = 0.02). The absence of catalase, the enzyme missing in *AaΔkatA* appears to hinder growth of Aa in mono and co-culture, suggesting that the capability to perform H_2O_2 detoxification inhibits growth of both *Aa* and *Sg* in mono and co-culture. Additionally, the equivalent growth of *Aa* and *AaΔlctD* in co-culture with *Sg* suggests that the benefits from co-culture with *Sg* extend beyond lactate catabolism. These results overall hint that the system may be reaching carrying capacity and the impact of specific metabolic exchange may not be identifiable based on number of viable cells alone. Chapters 2 and 3 showed that microbial interactions that impact physiology may not result in increased growth yield. Thus, I hypothesized that inhibiting metabolic exchange of L-lactate and H_2O_2 between *Aa* and *Sg* modulates aggregation, and spatial structure of the community.

4.2.2 Imaging *Aa* and *Sg* during infection.

To test this hypothesis, I imaged intact abscess infected with fluorescently labeled strains of *Aa* and *Sg* and collected 3D images using confocal microscopy. I used the same infections conditions as described in the previous section but given the limited number of

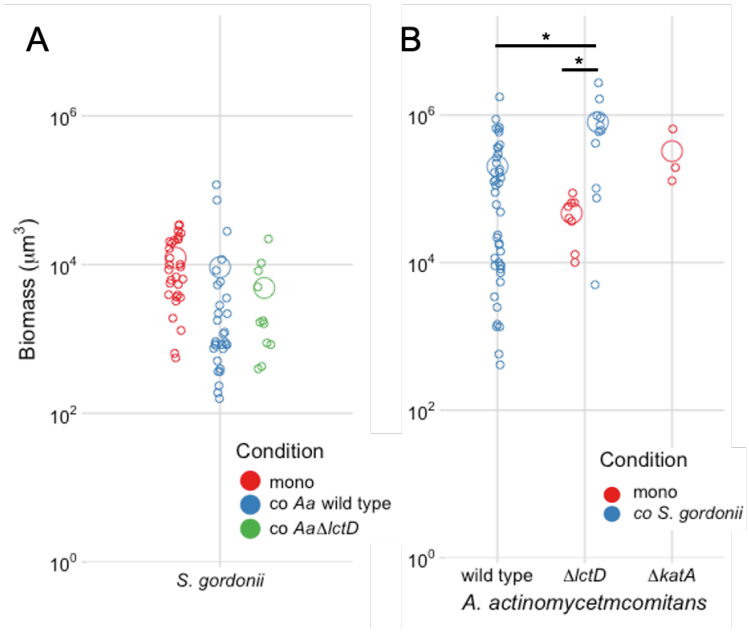

Figure 4-2 Fitness of *Sg* and Aa wild type, *AaΔlctD* and *AaΔkatA* in mono and coculture using confocal microscopy

(A) Observed biomass of *S. gordonii* in mono and co-culture with *Aa* wild type, *AaΔlctD* and *AaΔkatA.* Fitness of *Sg* did not change in mono-culture compared to co-culture with both *Aa* and *AaΔlctD*. (B) Observed biomass of *Aa* wild-type in co-culture with *Sg*, *AaΔlctD* in mono and co-culture with *Sg* and *AaΔkatA* in mono-culture. *Sg* increased growth of *AaΔlctD* 100-fold increase compared mono-culture. (* denotes *p*-value < 0.05, ANOVA one-way).

viable cells observed from *Aa* in mono-culture, I limited the image analysis of that strain to co-culture samples. Additionally, co-culture images with *Sg* and *AaΔkatA* have not been collected. Each abscess was extracted, placed on an imaging gasket with an antifade mountant to limit drift, and imaged at three or more different locations. The volume of abscess ranged from 20 to 30 mm^3, and confocal images were mostly 400 μm by 400 μm by 60 μm, or .01 mm3, so the imaging covered up to 1% of the total abscess volume.

The first task was to observe the extent to which images recapitulate the observations from CFUs. The fitness of *Sg* did not change in mono-culture compared to co-culture with both *Aa* and *AaΔlctD*, matching the findings from CFUs (Figure 4-2A). There were no images of *Aa* in mono-culture, but *Sg*-facilitated growth was observed in the *AaΔlctD*, showing a 100-fold increase in co-culture compared to *AaΔlctD* mono-culture, also matching the observation from CFU data (Figure 4-2B). These results indicate that while the images capture a small volume of the abscess, collectively represent the fitness effects observed.

4.2.3 *Aa* shifts *Sg* towards planktonic growth

The role of aggregation in bacterial physiology has been explained in previous chapters, but it can control antibiotic susceptibility and dormancy, thus it can be described as an indication for a shift in physiology. Other microbes shift from aggregates to planktonic cells in response to environmental changes, so I hypothesized that aggregation in the *Aa*-*Sg* model might also be impacted. To observe shifts in aggregation of *Sg* and *Aa* during infection, I classified the groups of bacteria from the confocal images according to their size. Objects up to 5 μm^3 were classified as planktonic cells and larger objects as

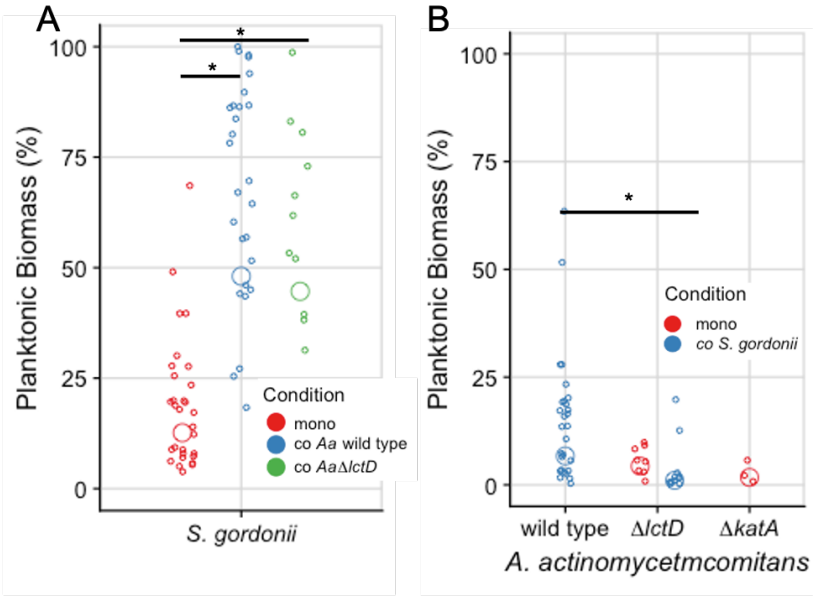

Figure 4-3 Contribution of planktonic cells to for *Aa* and *Sg* in mouse abscess.

(A) *Sg* planktonic cells biomass contribution in mono and co-culture with *Aa* and *AaΔlctD*. Planktonic cell biomass increased in mono- culture from 12% to 48% and 44% in co-culture with *Aa* and *AaΔlctD.* (B) Planktonic cells biomass contribution of *Aa* wild-type in co-culture with *Sg*, *AaΔlctD* in mono and co-culture with *Sg* and *AaΔkatA* in mono-culture. Planktonic cells of *Aa* in co-culture with *Sg* also showed a higher contribution to total biomass than *AaΔlctD* co-cultures with *Sg*. (* denotes *p*-value < 0.05, ANOVA one-way).

aggregates. I then calculated the contribution of planktonic cells to total biomass on each sample. While the total biomass of *Sg* is equivalent across conditions, its distribution is significantly shifted: 12% of biomass of *Sg* in mono-culture exists as planktonic cells compared to 48% and 44% in co-culture with *Aa* and *AaΔlctD* (Figure 4-3A) indicating that *Sg* may sense and respond to *Aa* without affecting its growth yield. Planktonic cells of *Aa* in co-culture with *Sg* also showed a higher contribution to total biomass than *AaΔlctD* co-cultures with *Sg*. (Figure 4-3B) These changes in aggregation are indicative of overall changes in physiology. Characterizing the distances between *Sg* and both *Aa* and *AaΔlctD* may further our understanding on different physiologies modulated by nutrient exchange.

4.2.4 L-lactate consumption drives *Aa* closer to *Sg*

While *Aa* and *AaΔlctD* reach the same yield during infection, the difference in aggregation suggests different physiology, primarily regarding nutritional strategy. Since *Aa* preferentially uses lactate to grow, I hypothesized that *Aa* would be found closer to *Sg* than *AaΔlctD* to gain access to *Sg*-released lactate. To test this hypothesis, I characterized the spatial organization of the co-culture images of *Sg* with *Aa* and *AaΔlctD* in the abscess using proportional occupancy (PO). In brief, PO characterizes the local environment surrounding a focus species in terms of presence of a target species at discrete distance intervals. The distance at which PO is the highest is defined as the enrichment distance. When *Sg* was used as focus surrounded by *Aa* or *AaΔlctD*, there was no difference in enrichment distance between *Aa* and *AaΔlctD*, and both centered at 9+/-2(Figure 4-4A). In the case of *Aa* or *AaΔlctD* surrounded by *Sg*, I found *Aa* to be closer to *Sg* than *AaΔlctD*, at 4 microns compared to 12(Figure 4-3B). This indicates that *Aa* may be positioning itself closer to *Sg* to feed on L-lactate released, while *AaΔlctD* is not. Additionally, it shows that

signatures of metabolic exchange between microbes can be observed *in vivo* by characterizing the spatial organization of the community.

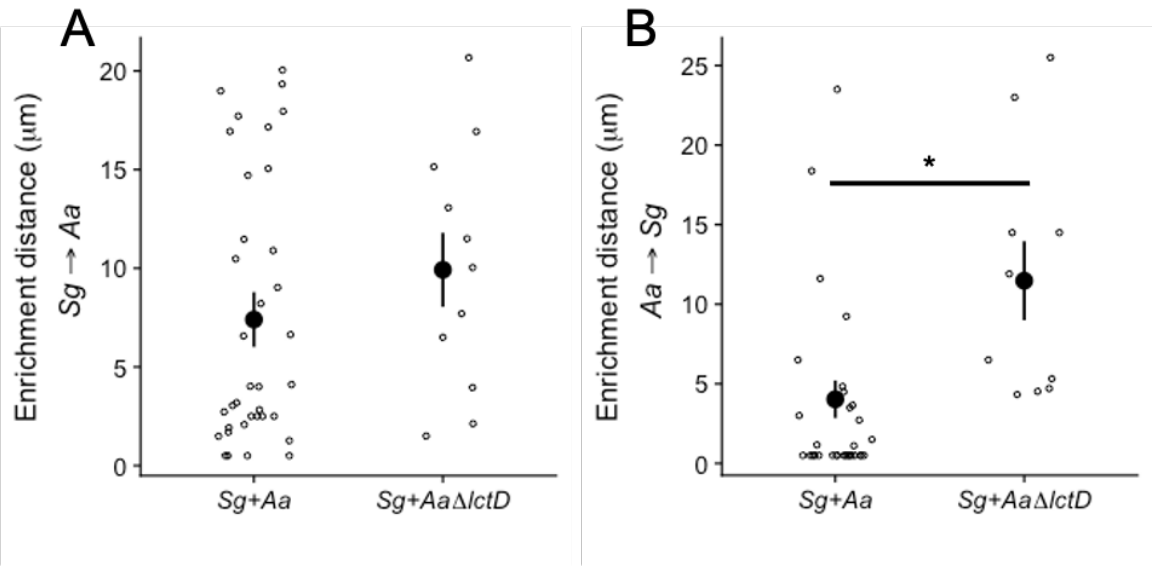

Figure 4-4 Enrichment distance between *Sg* and both *Aa* and *AaΔlctD.*

(A) Enrichment distance of *Aa* and *AaΔlctD* around *Sg*. There was no difference in enrichment distance between *Aa* and *AaΔlctD*, and both centered at 9+/-2. (B) Enrichment distance of *Sg* around *Aa* and *AaΔlctD*. Here, I found *Aa* to be closer to *Sg* than *AaΔlctD*, at 4 microns compared to 12. (* denotes p-value < 0.05, ANOVA one-way).

4.3 Discussion and conclusions

Sg reached a higher yield in the mouse co-culture with *AaΔkatA* compared to both mono and co-culture with *AaΔlctD*, but co-culture with *Aa* was not significantly different from either mono or co-culture with *AaΔkatA*. This suggests that *Sg* may benefit from presence of *Aa* only in the absence of catalase, indicating that H_2O_2 turnover may drive this phenotype. *Sg* does not benefit from oxygen since it cannot use it to respire but can instead convert it to H_2O_2. Released H_2O_2 can in turn inhibit growth of surrounding microbes, including other *Sg* cells, which are unable to decompose it. Hence, the net effect of oxygen to *Sg* may be inhibition. Presence of *Aa* may not affect local concentration of oxygen since it can both consume it for growth and release it using catalase to decompose H_2O_2. However, *AaΔkatA* would have the net effect of consumption of available oxygen, promoting growth of *Sg*. Imaging of *Sg* with *AaΔkatA* might also unravel this interaction since *Sg* responds to catalase in *Aa* by shifting to planktonic growth. These experiments will be performed in the near future.

The interruption of the O_2-H_2O_2 cycle may also benefit *Aa* because available oxygen would be coming exclusively from the environment, and not from the decomposition of H_2O_2. However, this reason alone is unlikely to promote growth in *AaΔkatA* up to levels near co-culture with *Sg*, and other mechanisms may be at play. Ultimately, the equivalent growth across all *Aa* strains in co-culture with *Sg* suggests the system has reached carrying capacity for *Aa*. This level of growth of *Aa* in co-culture has also been observed in other studies by the lab (83).

Previous data from our lab showed that catalase deficiency in a different strain of *Aa,* 624*,* does not benefit from co-culture with *Sg*. However, the fitness gain from co-culture with *Sg* in *Aa* 624 strain is 10% compared to the 5-log increase with wild-type strain used in this study, VT-1169. Although, Aa VT-1169 is significantly less fit in mono-culture than Aa 624, both strains reach equivalent numbers in the abscess model during co-culture with *Sg*, further suggesting a carrying capacity in that environment. This effect may also be responsible for lactate not being required for *Aa* fitness increase in co-culture as shown previously (70).

Another possible caveat of this study is the significant decrease of *Sg* observed biomass compared to *Aa*. There may be two explanations to this. First, while the aggregation of *Aa* and *Sg* during abscess is poorly understood, *in vitro* imaging shows Aa forms large aggregates, while *Sg* seldomly forms them and primarily forms chains of cells connecting at the poles. During imaging, I scanned the abscess looking for fluorescence, so the images could be biased towards capturing large aggregates of *Aa*, and against disseminated *Sg* cells. Because the images only capture a small part of the abscess volume, this may result in disseminated cells being undercounted compared to large aggregates. To test the impact of this bias I performed a linear model correlating planktonic cell contribution to the log of total biomass (Figure) for *Sg* in each image, but the correlation was negligible ($r^2 = 0.09$). While low aggregation may contribute to low biomass of *Sg*, I don't have enough data to show it. An alternative explanation may be *Sg* fluorescence signal is too low and current image analysis techniques can only identify a subset of the population. Ultimately, the fact that the overall trend from CFUs is maintained in the imaging data suggests that this effect impacts *Sg* equivalently across all conditions.

While spatial organization has been explored in the context of killing or inhibition (76), studies characterizing spatial organization resulting from nutrient exchange are limited. In this case, an *Aa* mutant unable to consume L-lactate was farther away from L-lactate releasing-*Sg* than the wild type. While the mechanism for this selective positioning is unclear since both microbes are non-motile, it nonetheless shows the potential value of using spatial organization to validate suspected metabolic interactions. Ultimately, using spatial structure characterization to show nutrient exchange provides a novel tool to identify nutritional interactions between community members.

4.4 Methods

4.4.1 Strains and Media

Streptococcus gordonii strain Challis DL1.1, *A. actinomycetemcomitans* strain VT1169, *A. actinomycetemcomitans* katA$^-$ and *A. actinomycetemcomitans* lctD$^-$ were used in this study. All cultures were grown in Tryptic Soy agar supplemented with 5% Yeast extract (TSAYE) overnight followed by overnight growth in Tryptic Soy broth supplemented with 5% Yeast extract (TSBYE) with antibiotics selecting for fluorescent plasmids and deletions. All *A. actinomycetemcomitans* strains were grown on 2 μg/mL vancomycin to maintain fluorescent plasmid. In addition to that *A. actinomycetemcomitans katA*$^-$, obtained from Stacy et al(83), was grown in 50 μg/ml Kanamycin and *A. actinomycetemcomitans lctD*$^-$ was obtained from Brown et al, (153) and was grown on 50 μg/mL Spectinomycin to maintain deletions. *S. gordonii* cultures were grown in TSBYE + 10 μg/mL erythromycin to maintain fluorescent plasmid. All cultures were grown at 37 °C

in a 5% CO2 atmosphere. *A. actinomycetemcomitans* were grown shaking at 250 rpm while *S. gordonii* remained static.

4.4.2 Mouse abscess model

Murine abscesses were generated essentially as described previously (70). Briefly, 6–8-week-old, female, Swiss Webster mice were anesthetized with flow of isoflurane according to protocol. The hair on inner part of the thigh to be infected of each mouse was shaved and disinfected with 70% ethanol. Mice were injected subcutaneously in the inner thigh with 10^8 CFU *A. actinomycetemcomitans*, *S. gordonii* or both. At 3 days post-infection, mice were euthanized, intact abscesses were harvested, and placed transferred to a 2 mL tube with metal beads and 1 ml of sterile PBS. Tissue was homogenized, serially diluted, and plated on Tryptic Soy agar supplemented with 5% Yeast extract (TSAYE) + 2 μg/mL vancomycin for *A. actinomycetemcomitans* enumeration and TSAYE + 10 μg/mL erythromycin for *S. gordonii* enumeration, to determine bacterial CFU/abscess.

4.4.3 Imaging of abscesses

Abscess imaging proceeded with a protocol similar to Chapter 3. Briefly, abscesses were placed in an CoverWell Imaging Chamber Gasket and two drops of ProLong Glass Antifade Mountant with NucBlue was added to prevent it from fading and minimize drift during imaging. Abscesses were incubated for 30 minutes at 4°C. Samples were then placed in the microscope with the skin of the abscess facing away from the objective. All images were acquired using a Zeiss LSM 880 CLSM utilizing Zen image-capture software with 3 different detectors. Detection of DsRed-expressing *S. aureus* cells was performed with an excitation wavelength centered at 587 nm and an emission wavelength centered at

610 nm. Detection of GFP-expressing cells was performed using an excitation wavelength centered at 488 nm and an emission wavelength centered at 509 nm. Detection of DAPI was performed exciting at 405 nm and detecting emission from 420 nm to 470 nm. All images were acquired using a 63X oil-immersion objective. The abscess was scanned for fluorescence signal and imaging began after centering in a region of interest. Images captured using tiles had 10% overlap and were later stitched using ZEN blue software.

4.4.4 Imaging analysis

Images were analyzed using the same tools used in Chapter 3. These images required an extra step of quality control. Images with less than 100 identified bacterial objects and with one object occupying more than 99% of the total sample biomass were discarded. Additionally, images were visually inspected for contamination from foreign objects, including mouse hair, and were also discarded.

CHAPTER 5. CONCLUSION AND FUTURE DIRECTIONS

Life is about context. Microbial communities control several aspects of life, ranging from flavor, texture, and aroma of cheese to human health. Understanding microbial life requires studying it in the right context. There were two primary approaches AppI used to maintain microbes in the right context: scale and environment. These two parameters are vital since microbial physiology is severely impacted by their size and their surroundings.

To study microbes in the right scale, I developed a computational framework to characterize several parameters from microscopy images of bacteria, primarily its spatial structure and organization. I chose to build those tools from "scratch", instead of using available software, because I wanted to understand every aspect of the process and ensure I make all the assumptions about the data handling. Additionally, I was able to customize the analysis to ask the specific questions I wanted to get answered. A key aspect of life and function in microbial communities is the interactions occurring between their members. Thus, one of the main goals of the tools I developed was to answer the question: How can we infer microbial interactions from microscopy images?

To apply these tools in the right environment, I imaged microbial communities in places where they perform a key aspect of life, infecting a host. The environments explored in this thesis; synthetic cystic fibrosis sputum, mouse chronic wound and thigh abscesses were chosen because they provide a stage for microbial communities to perform the functions that affect the host and may be influence by other community members.

The main finding of this thesis is that some interactions between microbes in a host or host-like environment correlate with features of community spatial structure that can be observed and quantified using the framework I developed. In this work explore the spatial structure resulting from both hostile and synergistic interactions.

In Chapter 2, I show how HQNO, an antimicrobial *P. aeruginosa* releases upon exposure to *S. aureus*, modulates the distance between these microbes, bringing them closer to each other in SCFM2. This was unexpected, since HQNO kills *S. aureus* in standard laboratory models, so we hypothesized HQNO would push them apart. However, in Chapter 3, I show that HQNO has the opposite impact on *P. aeruginosa* and *S. aureus* during infection in mouse chronic wound, increasing the distance between them. These results indicate that spatial structure associated with microbial interactions is specific to the environment and suggests that interactions between microbes may also be environment-specific.

In Chapter 4, I show how up to 40% of biomass of *S. gordonii* shifts from aggregate to planktonic cells in presence of *A. actinomycetemcomitans* during co-infection in a mouse abscess. Additionally, I showed that the distance between *A. actinomycetemcomitans* and *S. gordonii* is modulating by the ability of *Aa* to consume L-lactate released by *Sg*. These results show that nutrient exchange can modulate spatial organization in a microbial community and that the outcome of this interaction need not be increased growth yield.

One common theme on the results from all these studies is that none of the interaction outcomes from undisturbed communities involved a significant change in fitness. The only outcome involving fitness change was found in the increased susceptibility of *S. aureus* to

tobramycin in co-culture with *P. aeruginosa* compared to mono-culture. This may question how often are microbial "weapons" being deployed by pathogens against each other in an infection environment. It also shows that microbial interactions between pathogens can impact infection treatment without showing a shift in fitness. Finally, this opens the field for using spatial structure to characterize bacterial physiology and interactions.

The tools I developed for this work can be refined to better interrogate the spatial structure of microbial communities. One main avenue for this is incorporating the location and group size of the focal point in proportional occupancy (PO). Knowing the location of the focal point will decrease noise in the signal currently obtained from PO caused by focal points being partially or completely buried in the center of an aggregate. Knowing the size of focal point can identify the impact of aggregate size on microbial interactions and answer questions about physiology of aggregates compared to planktonic cells. After validating these tools, they can be implemented to characterize heterogeneity within a population. Ultimately this work is an invitation to rethink about what we can learn from observing bacteria at their scale in a relevant environment.

APPENDIX: SUPPLEMENTAL FIGURES

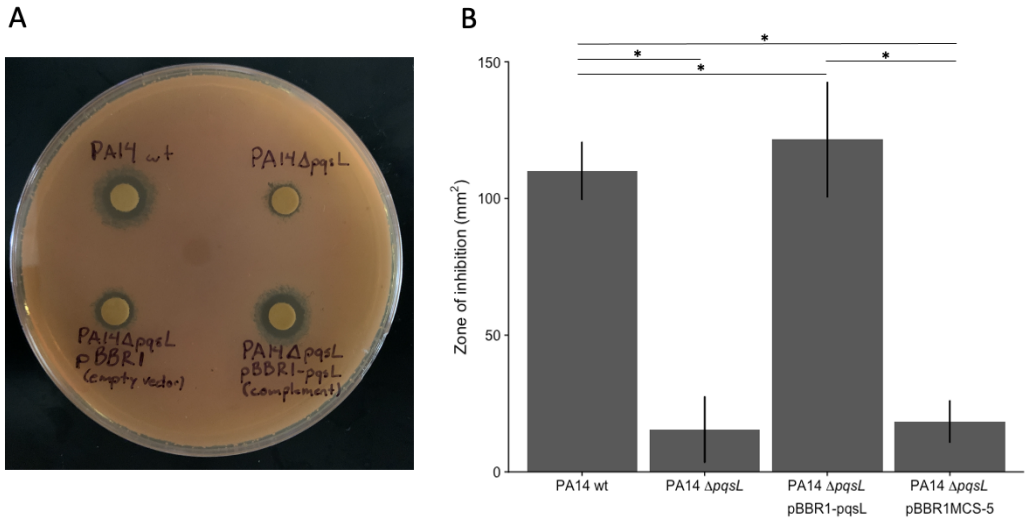

Figure S- 1 Expression of *pqsL* in *trans* restores S. aureus lytic activity in P. aeruginosa PA14 Δ*pqsL*.

(A) Image of BHI agar plate showing zones of inhibition formed by P. aeruginosa PA14, P. aeruginosa PA14 Δ*pqsL*, P. aeruginosa PA14 Δ*pqsL* carrying the complementation plasmid pBBR1-pqsL, and P. aeruginosa PA14 Δ*pqsL* carrying the control plasmid pBBR1MCS-5 (labeled pBBR1, empty vector) on an S. aureus LAC lawn. (B) Zone of inhibition (in square millimeters) produced by each strain. Error bars show standard deviations ($n = 4$). *, $P < 10^{-3}$ using a one-way analysis of variance (ANOVA) with Tukey's multiple-comparison test.

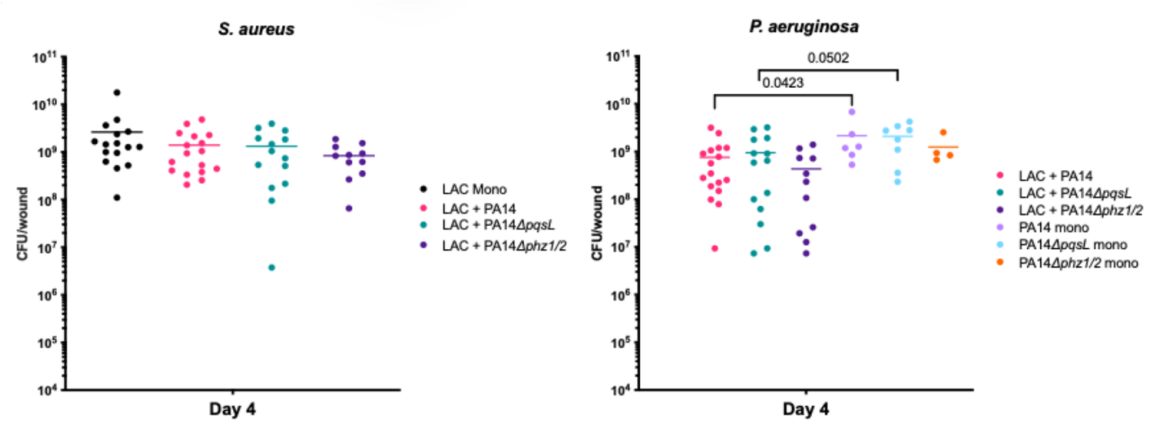

Figure S- 2 CFU counts for *P. aeruginosa* and *S. aureus* in mono and co-culture from mouse chronic wounds

Data collected by Carolyn Ibberson

REFERENCES

1. Stacy A, McNally L, Darch SE, Brown SP, Whiteley M. 2016. The biogeography of polymicrobial infection. Nature Reviews Microbiology 14:93-105.

2. Mark Welch JL, Hasegawa Y, Mcnulty NP, Gordon JI, Borisy GG. 2017. Spatial organization of a model 15-member human gut microbiota established in gnotobiotic mice. Proceedings of the National Academy of Sciences 114:E9105-E9114.

3. Flint HJ, Duncan SH, Scott KP, Louis P. 2007. Interactions and competition within the microbial community of the human colon: links between diet and health. Environmental Microbiology 9:1101-1111.

4. Widder S, Allen RJ, Pfeiffer T, Curtis TP, Wiuf C, Sloan WT, Cordero OX, Brown SP, Momeni B, Shou W, Kettle H, Flint HJ, Haas AF, Laroche B, Kreft J-U, Rainey PB, Freilich S, Schuster S, Milferstedt K, Van Der Meer JR, Groβkopf T, Huisman J, Free A, Picioreanu C, Quince C, Klapper I, Labarthe S, Smets BF, Wang H, Soyer OS. 2016. Challenges in microbial ecology: building predictive understanding of community function and dynamics. The ISME Journal 10:2557-2568.

5. Brogden KA, Guthmiller JM, Taylor CE. 2005. Human polymicrobial infections. The Lancet 365:253-255.

6. Dalton T, Dowd SE, Wolcott RD, Sun Y, Watters C, Griswold JA, Rumbaugh KP. 2011. An in vivo polymicrobial biofilm wound infection model to study interspecies interactions. PLoS One 6:e27317.

7. Cox CB, Moore PD. 2005. Biogeography: An Ecological and Evolutionary Approach doi:10.1080/10635150500541581. Blackwell Publishing.

8. Lomolino MV, Riddle BRC, Brown JHC. 2006. Biogeography. Sinauer Associates, Inc.

9. Martiny JBH, Bohannan BJM, Brown JH, Colwell RK, Fuhrman JA, Green JL, Horner-Devine MC, Kane M, Krumins JA, Kuske CR, Morin PJ, Naeem S, Øvreås L, Reysenbach A-L, Smith VH, Staley JT. 2006. Microbial biogeography: putting microorganisms on the map. Nature Reviews Microbiology 4:102-112.

10. Box EO. 1981. Predicting physiognomic vegetation types with climate variables. Vegetatio 45:127-139.

11. Prentice IC, Cramer W, Harrison SP, Leemans R, Monserud RA, Solomon AM. 1992. Special Paper: A Global Biome Model Based on Plant Physiology and Dominance, Soil Properties and Climate. Journal of Biogeography 19:117.

12. Ronquis ISF. 2004. Southern Hemisphere Biogeography Inferred by Event-Based Models: Plant versus Animal Patterns. Systematic Biology 53:216-243.

13. Toews DPL, Brelsford A. 2012. The biogeography of mitochondrial and nuclear discordance in animals. Molecular Ecology 21:3907-3930.

14. Hubbell SP. 1997. A unified theory of biogeography and relative species abundance and its application to tropical rain forests and coral reefs. Coral reefs 16:S9-S21.

15. Venter JC, Remington K, Heidelberg JF, Halpern AL, Rusch D, Eisen JA, Wu D, Paulsen I, Nelson KE, Nelson W. 2004. Environmental genome shotgun sequencing of the Sargasso Sea. science 304:66-74.

16. Øvreås L. 2000. Population and community level approaches for analysing microbial diversity in natural environments. Ecology Letters 3:236-251.

17. Becking LGMB. 1934. Geobiologie of inleiding tot de milieukunde. WP Van Stockum & Zoon.

18. Borisy GG, Valm AM. 2021. Spatial scale in analysis of the dental plaque microbiome. Periodontology 2000 86:97-112.

19. Wiens JA. 1989. Spatial Scaling in Ecology. Functional Ecology 3:385.

20. Levin SA. 1992. The problem of pattern and scale in ecology: the Robert H. MacArthur award lecture. Ecology 73:1943-1967.

21. Chave J. 2013. The problem of pattern and scale in ecology: what have we learned in 20 years? Ecology Letters 16:4-16.

22. Šizling AL, Storch D, Keil P. 2009. Rapoport's rule, species tolerances, and the latitudinal diversity gradient: geometric considerations. Ecology 90:3575-3586.

23. Holyoak M, Leibold MA, Mouquet N, Holt RD, Hoopes M. 2005. A framework for large scale community ecology. Metacommunities: spatial dynamics and ecological communities The University of Chicago Press, Chicago:1-31.

24. Green J, Bohannan BJ. 2006. Spatial scaling of microbial biodiversity. Trends in ecology & evolution 21:501-507.

25. Connolly SR, Macneil MA, Caley MJ, Knowlton N, Cripps E, Hisano M, Thibaut LM, Bhattacharya BD, Benedetti-Cecchi L, Brainard RE, Brandt A, Bulleri F, Ellingsen KE, Kaiser S, Kroncke I, Linse K, Maggi E, O'Hara TD, Plaisance L, Poore GCB, Sarkar SK, Satpathy KK, Schuckel U, Williams A, Wilson RS. 2014.

Commonness and rarity in the marine biosphere. Proceedings of the National Academy of Sciences 111:8524-8529.

26. Magurran AE, Henderson PA. 2003. Explaining the excess of rare species in natural species abundance distributions. Nature 422:714-716.

27. Preston FW. 1948. The Commonness, And Rarity, of Species. Ecology 29:254-283.

28. Sugihara G, Bersier L-F, Southwood TRE, Pimm SL, May RM. 2003. Predicted correspondence between species abundances and dendrograms of niche similarities. Proceedings of the National Academy of Sciences 100:5246-5251.

29. Ley RE, Turnbaugh PJ, Klein S, Gordon JI. 2006. Human gut microbes associated with obesity. nature 444:1022-1023.

30. Dewhirst FE, Chen T, Izard J, Paster BJ, Tanner AC, Yu W-H, Lakshmanan A, Wade WG. 2010. The human oral microbiome. Journal of bacteriology 192:5002-5017.

31. Dawson W, Hör J, Egert M, van Kleunen M, Pester M. 2017. A small number of low-abundance bacteria dominate plant species-specific responses during rhizosphere colonization. Frontiers in microbiology 8:975.

32. Bickel S, Or D. 2021. The chosen few—variations in common and rare soil bacteria across biomes. The ISME Journal doi:10.1038/s41396-021-00981-3.

33. Nemergut DR, Schmidt SK, Fukami T, O'Neill SP, Bilinski TM, Stanish LF, Knelman JE, Darcy JL, Lynch RC, Wickey P. 2013. Patterns and processes of microbial community assembly. Microbiology and Molecular Biology Reviews 77:342-356.

34. Brown JH. 1984. On the relationship between abundance and distribution of species. The american naturalist 124:255-279.

35. Crone S, Vives-Flórez M, Kvich L, Saunders AM, Malone M, Nicolaisen MH, Martínez-García E, Rojas-Acosta C, Catalina Gomez-Puerto M, Calum H, Whiteley M, Kolter R, Bjarnsholt T. 2020. The environmental occurrence of

Pseudomonas aeruginosa. APMIS 128:220-231.

36. Zemanick ET, Sagel SD, Harris JK. 2011. The airway microbiome in cystic fibrosis and implications for treatment. Current Opinion in Pediatrics 23:319-324.

37. Tipton CD, Mathew ME, Wolcott RA, Wolcott RD, Kingston T, Phillips CD. 2017. Temporal dynamics of relative abundances and bacterial succession in chronic wound communities. Wound Repair and Regeneration 25:673-679.

38. Loesche M, Gardner SE, Kalan L, Horwinski J, Zheng Q, Hodkinson BP, Tyldsley AS, Franciscus CL, Hillis SL, Mehta S, Margolis DJ, Grice EA. 2017. Temporal Stability in Chronic Wound Microbiota Is Associated With Poor Healing. Journal of Investigative Dermatology 137:237-244.

39. Turing AM. 1990. The chemical basis of morphogenesis. Bulletin of mathematical biology 52:153-197.

40. Nakamasu A, Takahashi G, Kanbe A, Kondo S. 2009. Interactions between zebrafish pigment cells responsible for the generation of Turing patterns. Proceedings of the National Academy of Sciences 106:8429-8434.

41. Sick S, Reinker S, Timmer J, Schlake T. 2006. WNT and DKK determine hair follicle spacing through a reaction-diffusion mechanism. Science 314:1447-1450.

42. Jiang T-X, Jung H-S, Widelitz RB, Chuong C-M. 1999. Self-organization of periodic patterns by dissociated feather mesenchymal cells and the regulation of size, number and spacing of primordia. Development 126:4997-5009.

43. Bánsági T, Vanag VK, Epstein IR. 2011. Tomography of reaction-diffusion microemulsions reveals three-dimensional Turing patterns. Science 331:1309-1312.

44. Karig D, Martini KM, Lu T, Delateur NA, Goldenfeld N, Weiss R. 2018. Stochastic Turing patterns in a synthetic bacterial population. Proceedings of the National Academy of Sciences 115:6572-6577.

45. Koch AL. 1990. Diffusion the crucial process in many aspects of the biology of bacteria. Advances in microbial ecology:37-70.

46. Jepson A, Martinez VA, Schwarz-Linek J, Morozov A, Poon WC. 2013. Enhanced diffusion of nonswimmers in a three-dimensional bath of motile bacteria. Physical Review E 88:041002.

47. Fuqua WC, Winans SC, Greenberg EP. 1994. Quorum sensing in bacteria: the LuxR-LuxI family of cell density-responsive transcriptional regulators. Journal of bacteriology 176:269-275.

48. Nekola JC, White PS. 1999. The distance decay of similarity in biogeography and ecology. Journal of biogeography 26:867-878.

49. Zhang M, Sheffield T, Zhan X, Li Q, Yang DM, Wang Y, Wang S, Xie Y, Wang T, Xiao G. 2020. Spatial molecular profiling: platforms, applications and analysis tools. Brief Bioinform doi:10.1093/bib/bbaa145.

50. Cho J-C, Tiedje JM. 2000. Biogeography and degree of endemicity of fluorescent Pseudomonas strains in soil. Applied and environmental microbiology 66:5448-5456.

51. Hillebrand H, Watermann F, Karez R, Berninger U-G. 2001. Differences in species richness patterns between unicellular and multicellular organisms. Oecologia 126:114-124.

52. Listgarten MA. 1994. The structure of dental plaque. Periodontology 2000 5:52-65.

53. Adriaens PA, Edwards CA, De Boever JA, Loesche WJ. 1988. Ultrastructural observations on bacterial invasion in cementum and radicular dentin of periodontally diseased human teeth. Journal of periodontology 59:493-503.

54. Valm AM, Welch JLM, Rieken CW, Hasegawa Y, Sogin ML, Oldenbourg R, Dewhirst FE, Borisy GG. 2011. Systems-level analysis of microbial community organization through combinatorial labeling and spectral imaging. Proceedings of the National Academy of Sciences 108:4152-4157.

55. Kim D, Barraza JP, Arthur RA, Hara A, Lewis K, Liu Y, Scisci EL, Hajishengallis E, Whiteley M, Koo H. 2020. Spatial mapping of polymicrobial communities reveals a precise biogeography associated with human dental caries. Proceedings of the National Academy of Sciences 117:12375-12386.

56. Watnick P, Kolter R. 2000. Biofilm, city of microbes. Journal of bacteriology 182:2675-2679.

57. O'Toole G, Kaplan HB, Kolter R. 2000. Biofilm formation as microbial development. Annual Reviews in Microbiology 54:49-79.

58. Hall-Stoodley L, Stoodley P. 2009. Evolving concepts in biofilm infections. Cellular microbiology 11:1034-1043.

59. Darch SE, Kragh KN, Abbott EA, Bjarnsholt T, Bull JJ, Whiteley M. 2017. Phage Inhibit Pathogen Dissemination by Targeting Bacterial Migrants in a Chronic Infection Model. mBio 8:e00240-17.

60. Bjarnsholt T, Jensen PØ, Fiandaca MJ, Pedersen J, Hansen CR, Andersen CB, Pressler T, Givskov M, Høiby N. 2009. Pseudomonas aeruginosa biofilms in the respiratory tract of cystic fibrosis patients. Pediatric pulmonology 44:547-558.

61. Darch SE, Simoska O, Fitzpatrick M, Barraza JP, Stevenson KJ, Bonnecaze RT, Shear JB, Whiteley M. 2018. Spatial determinants of quorum signaling in a Pseudomonas aeruginosa infection model. Proceedings of the National Academy of Sciences 115:4779-4784.

62. Welch JLM, Rossetti BJ, Rieken CW, Dewhirst FE, Borisy GG. 2016. Biogeography of a human oral microbiome at the micron scale. Proceedings of the National Academy of Sciences 113:E791-E800.

63. Grimes DJ. 2006. Koch's postulates-then and now. Microbe-American Society for Microbiology 1:223.

64. Falkow S. 1988. Molecular Koch's postulates applied to microbial pathogenicity. Reviews of infectious diseases:S274-S276.

65. Murray JL, Connell JL, Stacy A, Turner KH, Whiteley M. 2014. Mechanisms of synergy in polymicrobial infections. Journal of Microbiology 52:188-199.

66. Faust K, Raes J. 2012. Microbial interactions: from networks to models. Nature Reviews Microbiology 10:538-550.

67. Darch SE, Ibberson CB, Whiteley M. 2017. Evolution of bacterial “frenemies”. MBio 8:e00675-17.

68. Radlinski L, Rowe SE, Kartchner LB, Maile R, Cairns BA, Vitko NP, Gode CJ, Lachiewicz AM, Wolfgang MC, Conlon BP. 2017. Pseudomonas aeruginosa exoproducts determine antibiotic efficacy against Staphylococcus aureus. PLOS Biology 15:e2003981.

69. Machan ZA, Taylor GW, Pitt TL, Cole PJ, Wilson R. 1992. 2-Heptyl-4-hydroxyquinoline N-oxide, an antistaphylococcal agent produced by Pseudomonas aeruginosa. J Antimicrob Chemother 30:615-23.

70. Ramsey MM, Rumbaugh KP, Whiteley M. 2011. Metabolite Cross-Feeding Enhances Virulence in a Model Polymicrobial Infection. PLoS Pathogens 7:e1002012.

71. Brown SA, Whiteley M. 2007. A Novel Exclusion Mechanism for Carbon Resource Partitioning in Aggregatibacter actinomycetemcomitans. Journal of Bacteriology 189:6407-6414.

72. Stacy A, Fleming D, Lamont RJ, Rumbaugh KP, Whiteley M. 2016. A Commensal Bacterium Promotes Virulence of an Opportunistic Pathogen via Cross-Respiration. mBio 7:e00782-16.

73. Green ER, Mecsas J. 2016. Bacterial Secretion Systems: An Overview. Microbiology Spectrum 4:215-239.

74. Hayes CS, Koskiniemi S, Ruhe ZC, Poole SJ, Low DA. 2014. Mechanisms and Biological Roles of Contact-Dependent Growth Inhibition Systems. Cold Spring Harbor Perspectives in Medicine 4:a010025-a010025.

75. Pukatzki S, Ma AT, Revel AT, Sturtevant D, Mekalanos JJ. 2007. Type VI secretion system translocates a phage tail spike-like protein into target cells where it cross-links actin. Proceedings of the National Academy of Sciences 104:15508-15513.

76. Mcnally L, Bernardy E, Thomas J, Kalziqi A, Pentz J, Brown SP, Hammer BK, Yunker PJ, Ratcliff WC. 2017. Killing by Type VI secretion drives genetic phase separation and correlates with increased cooperation. Nature Communications 8:14371.

77. Tagg JR, Dajani AS, Wannamaker LW. 1976. Bacteriocins of gram-positive bacteria. Bacteriological reviews 40:722-756.

78. Reeves P. 1965. The bacteriocins. Bacteriological reviews 29:24-45.

79. Cascales E, Buchanan SK, Duché D, Kleanthous C, LloubèS R, Postle K, Riley M, Slatin S, Cavard DL. 2007. Colicin Biology. Microbiology and Molecular Biology Reviews 71:158-229.

80. Korgaonkar A, Trivedi U, Rumbaugh KP, Whiteley M. 2013. Community surveillance enhances Pseudomonas aeruginosa virulence during polymicrobial infection. Proceedings of the National Academy of Sciences 110:1059-1064.

81. Lightbown J, Jackson F. 1956. Inhibition of cytochrome systems of heart muscle and certain bacteria by the antagonists of dihydrostreptomycin: 2-alkyl-4-hydroxyquinoline N-oxides. Biochemical Journal 63:130-137.

82. Foundation C. 2015. 2014 Annual Data Report. Cystic Fibrosis Foundation Patient Registry.

83. Stacy A, Everett J, Jorth P, Trivedi U, Rumbaugh KP, Whiteley M. 2014. Bacterial fight-and-flight responses enhance virulence in a polymicrobial infection. Proceedings of the National Academy of Sciences 111:7819-7824.

84. Guerinot ML. 1994. Microbial iron transport. Annual review of microbiology 48:743-772.

85. Ratledge C, Dover LG. 2000. Iron metabolism in pathogenic bacteria. Annual reviews in microbiology 54:881-941.

86. Harrison F, Paul J, Massey RC, Buckling A. 2008. Interspecific competition and siderophore-mediated cooperation in Pseudomonas aeruginosa. The ISME journal 2:49-55.

87. Yanni D, Márquez-Zacarías P, Yunker PJ, Ratcliff WC. 2019. Drivers of Spatial Structure in Social Microbial Communities. Current Biology 29:R545-R550.

88. Kümmerli R, Griffin AS, West SA, Buckling A, Harrison F. 2009. Viscous medium promotes cooperation in the pathogenic bacterium

Pseudomonas aeruginosa. Proceedings of the Royal Society B: Biological Sciences 276:3531-3538.

89. Hol FJH, Galajda P, Nagy K, Woolthuis RG, Dekker C, Keymer JE. 2013. Spatial Structure Facilitates Cooperation in a Social Dilemma: Empirical Evidence from a Bacterial Community. PLoS ONE 8:e77042.

90. Cendra MDM, Blanco-Cabra N, Pedraz L, Torrents E. 2019. Optimal environmental and culture conditions allow the in vitro coexistence of Pseudomonas aeruginosa and Staphylococcus aureus in stable biofilms. Scientific Reports 9.

91. ÖSterberg SKÅ, Sudo SZ, Folke LE. 1976. Microbial succession in subgingival plaque of man. Journal of periodontal research 11:243-255.

92. Dige I, Raarup M, Nyengaard J, Kilian M, Nyvad B. 2009. Actinomyces naeslundii in initial dental biofilm formation. Microbiology 155:2116-2126.

93. Kolenbrander PE, Palmer Jr RJ, Rickard AH, Jakubovics NS, Chalmers NI, Diaz PI. 2006. Bacterial interactions and successions during plaque development. Periodontology 2000 42:47-79.

94. Griffiths EC, Pedersen AB, Fenton A, Petchey OL. 2011. The nature and consequences of coinfection in humans. Journal of Infection 63:200-206.

95. Smith H. 1982. The role of microbial interactions in infectious disease. Philosophical Transactions of the Royal Society of London B, Biological Sciences 297:551-561.

96. Knapp EA, Fink AK, Goss CH, Sewall A, Ostrenga J, Dowd C, Elbert A, Petren KM, Marshall BC. 2016. The Cystic Fibrosis Foundation Patient Registry. Design and methods of a national observational disease registry. Annals of the American Thoracic Society 13:1173-1179.

97. Trivedi U, Parameswaran S, Armstrong A, Burgueno-Vega D, Griswold J, Dissanaike S, Rumbaugh KP. 2014. Prevalence of multiple antibiotic resistant infections in diabetic versus nondiabetic wounds. Journal of pathogens 2014.

98. Hubert D, Réglier-Poupet H, Sermet-Gaudelus I, Ferroni A, Le Bourgeois M, Burgel P-R, Serreau R, Dusser D, Poyart C, Coste J. 2013. Association between Staphylococcus aureus alone or combined with Pseudomonas aeruginosa and the clinical condition of patients with cystic fibrosis. Journal of Cystic Fibrosis 12:497-503.

99. Emerson J, Rosenfeld M, McNamara S, Ramsey B, Gibson RL. 2002. Pseudomonas aeruginosa and other predictors of mortality and morbidity in young children with cystic fibrosis. Pediatr Pulmonol 34:91-100.

100. Zhao J, Schloss PD, Kalikin LM, Carmody LA, Foster BK, Petrosino JF, Cavalcoli JD, VanDevanter DR, Murray S, Li JZ. 2012. Decade-long bacterial community

dynamics in cystic fibrosis airways. Proceedings of the National Academy of Sciences 109:5809-5814.

101. Goss CH, Muhlebach MS. 2011. Staphylococcus aureus and MRSA in cystic fibrosis. Journal of Cystic fibrosis 10:298-306.

102. Cigana C, Bianconi I, Baldan R, De Simone M, Riva C, Sipione B, Rossi G, Cirillo DM, Bragonzi A. 2017. Staphylococcus aureus Impacts Pseudomonas aeruginosa Chronic Respiratory Disease in Murine Models. The Journal of Infectious Diseases 217:933-942.

103. Ibberson CB, Stacy A, Fleming D, Dees JL, Rumbaugh K, Gilmore MS, Whiteley M. 2017. Co-infecting microorganisms dramatically alter pathogen gene essentiality during polymicrobial infection. Nature Microbiology 2:17079.

104. Mashburn LM, Jett AM, Akins DR, Whiteley M. 2005. Staphylococcus aureus serves as an iron source for Pseudomonas aeruginosa during in vivo coculture. Journal of bacteriology 187:554-566.

105. Millette G, Langlois J-P, Brouillette E, Frost EH, Cantin A, Malouin F. 2019. Despite antagonism in vitro, Pseudomonas aeruginosa enhances Staphylococcus aureus colonization in a murine lung infection model. Frontiers in microbiology 10:2880.

106. Kessler E, Safrin M, Olson J, Ohman D. 1993. Secreted LasA of Pseudomonas aeruginosa is a staphylolytic protease. The Journal of biological chemistry 268:7503-7508.

107. Mashburn LM, Whiteley M. 2005. Membrane vesicles traffic signals and facilitate group activities in a prokaryote. Nature 437:422-5.

108. Niggli S, Kummerli R. 2020. Strain background, species frequency and environmental conditions are important in determining population dynamics and species co-existence between Pseudomonas aeruginosa and Staphylococcus aureus. Appl Environ Microbiol doi:10.1128/AEM.00962-20.

109. Palmer KL, Aye LM, Whiteley M. 2007. Nutritional Cues Control Pseudomonas aeruginosa Multicellular Behavior in Cystic Fibrosis Sputum. Journal of Bacteriology 189:8079-8087.

110. Palmer KL, Mashburn LM, Singh PK, Whiteley M. 2005. Cystic fibrosis sputum supports growth and cues key aspects of Pseudomonas aeruginosa physiology. Journal of bacteriology 187:5267-5277.

111. Zoe A. Macnan GWT, Tyrone L. Pttt, Peter J. Cole and Robert Wilson. 1992. Heptyl-4-hydroxyquinoline N-oxide, an antistaphylococcal agent produced by Pseudomonas aeruginosa. Journal of Antimicrobial Chemotherapy.

112. Orazi G, O'Toole GA. 2017. Pseudomonas aeruginosa Alters Staphylococcus aureus Sensitivity to Vancomycin in a Biofilm Model of Cystic Fibrosis Infection. mBio 8.

113. Orazi G, Ruoff KL, O'Toole GA. 2019. Pseudomonas aeruginosa Increases the Sensitivity of Biofilm-Grown Staphylococcus aureus to Membrane-Targeting Antiseptics and Antibiotics. mBio 10.

114. Fugère A, Lalonde Séguin D, Mitchell G, Déziel E, Dekimpe V, Cantin AM, Frost E, Malouin F. 2014. Interspecific Small Molecule Interactions between Clinical Isolates of Pseudomonas aeruginosa and Staphylococcus aureus from Adult Cystic Fibrosis Patients. PLoS ONE 9:e86705.

115. Park JH, Lee JH, Cho MH, Herzberg M, Lee J. 2012. Acceleration of protease effect on Staphylococcus aureus biofilm dispersal. FEMS Microbiol Lett 335:31-8.

116. Castric PA. 1975. Hydrogen cyanide, a secondary metabolite of Pseudomonas aeruginosa. Can J Microbiol 21:613-18.

117. Hassan HM, Fridovich I. 1980. Mechanism of the antibiotic action pyocyanine. Journal of bacteriology 141:156-163.

118. Mitchell G, Séguin D, Asselin A-E, Déziel E, Cantin AM, Frost EH, Michaud S, Malouin F. 2010. Staphylococcus aureus sigma B-dependent emergence of small-colony variants and biofilm production following exposure to Pseudomonas aeruginosa 4-hydroxy-2-heptylquinoline-N-oxide. BMC Microbiology 10:33.

119. Filkins LM, Graber JA, Olson DG, Dolben EL, Lynd LR, Bhuju S, O'Toole GA. 2015. Coculture of Staphylococcus aureus with Pseudomonas aeruginosa Drives S. aureus towards Fermentative Metabolism and Reduced Viability in a Cystic Fibrosis Model. Journal of Bacteriology 197:2252-2264.

120. Hoffman LR, Déziel E, d'Argenio DA, Lépine F, Emerson J, McNamara S, Gibson RL, Ramsey BW, Miller SI. 2006. Selection for Staphylococcus aureus small-colony variants due to growth in the presence of Pseudomonas aeruginosa. Proceedings of the National Academy of Sciences 103:19890-19895.

121. Jiang X, Zerfaß C, Feng S, Eichmann R, Asally M, Schäfer P, Soyer OS. 2018. Impact of spatial organization on a novel auxotrophic interaction among soil microbes. The ISME Journal 12:1443-1456.

122. Ratzke C, Gore J. 2016. Self-organized patchiness facilitates survival in a cooperatively growing Bacillus subtilis population. Nature Microbiology 1:16022.

123. Limoli DH, Whitfield GB, Kitao T, Ivey ML, Davis MR, Grahl N, Hogan DA, Rahme LG, Howell PL, O'Toole GA, Goldberg JB. 2017. Pseudomonas aeruginosa Alginate Overproduction Promotes Coexistence with Staphylococcus aureus in a Model of Cystic Fibrosis Respiratory Infection. mBio 8:e00186-17.

124. Ibberson CB, Whiteley M. 2019. The Staphylococcus aureus Transcriptome during Cystic Fibrosis Lung Infection. mBio 10.

125. Cornforth DM, Diggle FL, Melvin JA, Bomberger JM, Whiteley M. 2020. Quantitative Framework for Model Evaluation in Microbiology Research Using Pseudomonas aeruginosa and Cystic Fibrosis Infection as a Test Case. mBio 11.

126. Turner KH, Wessel AK, Palmer GC, Murray JL, Whiteley M. 2015. Essential genome of Pseudomonas aeruginosa in cystic fibrosis sputum. Proceedings of the National Academy of Sciences 112:4110-4115.

127. Briaud P, Camus L, Bastien S, Doleans-Jordheim A, Vandenesch F, Moreau K. 2019. Coexistence with Pseudomonas aeruginosa alters Staphylococcus aureus transcriptome, antibiotic resistance and internalization into epithelial cells. Sci Rep 9:16564.

128. Limoli DH, Warren EA, Yarrington KD, Donegan NP, Cheung AL, O'Toole GA. 2019. Interspecies interactions induce exploratory motility in Pseudomonas aeruginosa. Elife 8.

129. Cornforth DM, Dees JL, Ibberson CB, Huse HK, Mathiesen IH, Kirketerp-Moller K, Wolcott RD, Rumbaugh KP, Bjarnsholt T, Whiteley M. 2018. Pseudomonas aeruginosa transcriptome during human infection. Proc Natl Acad Sci U S A 115:E5125-E5134.

130. Pallett R, Leslie LJ, Lambert PA, Milic I, Devitt A, Marshall LJ. 2019. Anaerobiosis influences virulence properties of Pseudomonas aeruginosa cystic fibrosis isolates and the interaction with Staphylococcus aureus. Sci Rep 9:6748.

131. Schertzer JW, Brown SA, Whiteley M. 2010. Oxygen levels rapidly modulate Pseudomonas aeruginosa social behaviours via substrate limitation of PqsH. Mol Microbiol 77:1527-38.

132. Bjarnsholt T, Alhede M, Alhede M, Eickhardt-Sorensen SR, Moser C, Kuhl M, Jensen PO, Hoiby N. 2013. The in vivo biofilm. Trends Microbiol 21:466-74.

133. DePas WH, Starwalt-Lee R, Van Sambeek L, Ravindra Kumar S, Gradinaru V, Newman DK. 2016. Exposing the Three-Dimensional Biogeography and Metabolic States of Pathogens in Cystic Fibrosis Sputum via Hydrogel Embedding, Clearing, and rRNA Labeling. mBio 7.

134. Kragh KN, Alhede M, Jensen PO, Moser C, Scheike T, Jacobsen CS, Seier Poulsen S, Eickhardt-Sorensen SR, Trostrup H, Christoffersen L, Hougen HP, Rickelt LF, Kuhl M, Hoiby N, Bjarnsholt T. 2014. Polymorphonuclear leukocytes restrict growth of Pseudomonas aeruginosa in the lungs of cystic fibrosis patients. Infect Immun 82:4477-86.

135. Rickard AH, Gilbert P, High NJ, Kolenbrander PE, Handley PS. 2003. Bacterial coaggregation: an integral process in the development of multi-species biofilms. Trends in microbiology 11:94-100.

136. Palmer KL, Brown SA, Whiteley M. 2007. Membrane-bound nitrate reductase is required for anaerobic growth in cystic fibrosis sputum. J Bacteriol 189:4449-55.

137. Speare L, Smith S, Salvato F, Kleiner M, Septer AN. 2020. Environmental Viscosity Modulates Interbacterial Killing during Habitat Transition. mBio 11.

138. Davies DG. 1998. The Involvement of Cell-to-Cell Signals in the Development of a Bacterial Biofilm. Science 280:295-298.

139. Ibberson CB, Parlet CP, Kwiecinski J, Crosby HA, Meyerholz DK, Horswill AR. 2016. Hyaluronan Modulation Impacts Staphylococcus aureus Biofilm Infection. 84:1917-1929.

140. Chung CT, Niemela SL, Miller RH. 1989. One-step preparation of competent Escherichia coli: transformation and storage of bacterial cells in the same solution. Proceedings of the National Academy of Sciences 86:2172-2175.

141. Whiteley M, Lee KM, Greenberg EP. 1999. Identification of genes controlled by quorum sensing in Pseudomonas aeruginosa. Proc Natl Acad Sci U S A 96:13904-9.

142. D'Argenio DA, Calfee MW, Rainey PB, Pesci EC. 2002. Autolysis and Autoaggregation in Pseudomonas aeruginosa Colony Morphology Mutants. Journal of Bacteriology 184:6481-6489.

143. Kovach ME, Elzer PH, Hill DS, Robertson GT, Farris MA, Roop RM, 2nd, Peterson KM. 1995. Four new derivatives of the broad-host-range cloning vector pBBR1MCS, carrying different antibiotic-resistance cassettes. Gene 166:175-6.

144. Otsu N. 1979. A threshold selection method from gray-level histograms. IEEE Trans Sys Man Cyber 9:62-66.

145. Cigana C, Bianconi I, Baldan R, De Simone M, Riva C, Sipione B, Rossi G, Cirillo DM, Bragonzi A. 2018. Staphylococcus aureus impacts Pseudomonas aeruginosa chronic respiratory disease in murine models. The Journal of infectious diseases 217:933-942.

146. Biswas L, Biswas R, Schlag M, Bertram R, Götz F. 2009. Small-colony variant selection as a survival strategy for Staphylococcus aureus in the presence of Pseudomonas aeruginosa. Applied and environmental microbiology 75:6910-6912.

147. Chua SL, Liu Y, Yam JKH, Chen Y, Vejborg RM, Tan BGC, Kjelleberg S, Tolker-Nielsen T, Givskov M, Yang L. 2014. Dispersed cells represent a distinct stage in

the transition from bacterial biofilm to planktonic lifestyles. Nature communications 5:1-12.

148. Rumbaugh KP, Sauer K. 2020. Biofilm dispersion. Nature Reviews Microbiology 18:571-586.

149. Crosby HA, Kwiecinski J, Horswill AR. 2016. Staphylococcus aureus Aggregation and Coagulation Mechanisms, and Their Function in Host–Pathogen Interactions, p 1-41, Advances in Applied Microbiology doi:10.1016/bs.aambs.2016.07.018. Elsevier.

150. Cornforth DM, Dees JL, Ibberson CB, Huse HK, Mathiesen IH, Kirketerp-Møller K, Wolcott RD, Rumbaugh KP, Bjarnsholt T, Whiteley M. 2018. Pseudomonas aeruginosa transcriptome during human infection. Proceedings of the National Academy of Sciences 115:E5125-E5134.

151. Gendron R, Grenier D, Maheu-Robert L-F. 2000. The oral cavity as a reservoir of bacterial pathogens for focal infections. Microbes and infection 2:897-906.

152. Barnard JP, Stinson MW. 1999. Influence of environmental conditions on hydrogen peroxide formation by Streptococcus gordonii. Infection and immunity 67:6558-6564.

153. Brown SA, Whiteley M. 2009. Characterization of the L-Lactate Dehydrogenase from Aggregatibacter actinomycetemcomitans. PLoS ONE 4:e7864.